Nanoscale

Accepted Manuscript

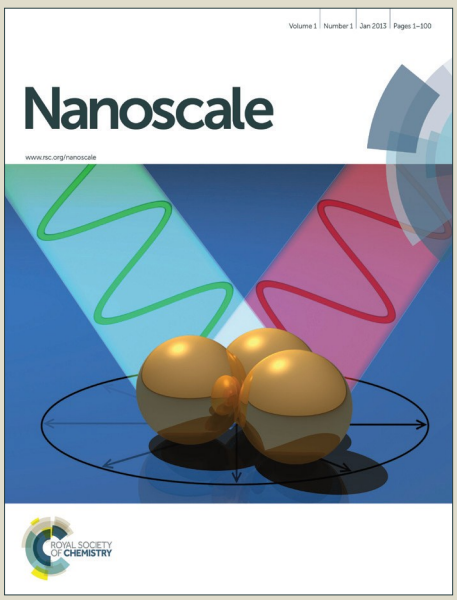

ROYAL SOCIETY OF CHEMISTRY

www.rsc.org/nanoscale

An overview on emerging photoelectrochemical self-powered ultraviolet photodetectors

Jinyuan Zhou†,*, Lulu Chen†, Youqing Wang†, Yongmin He, Xiaojun Pan, Erqing Xie*

School of Physical Science and Technology, Lanzhou University, Lanzhou 730000, Gansu, P.R. China

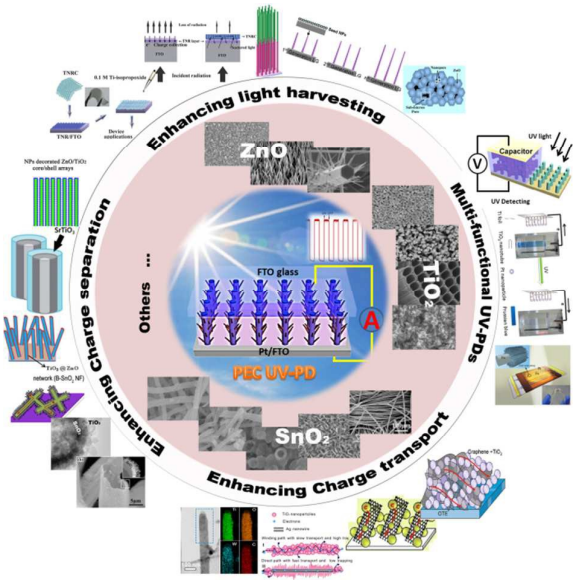

*Corresponding authors. Tel./Fax: +86 931 8915895. E-mail addresses: zhoujy@lzu.edu.cn; xieeq@lzu.edu.cn.

†These authors contributed equally to this work.

Abstract

In recent years, as a new member of ultraviolet photodetectors (UV-PDs), photoelectrochemical UV-PDs (PEC UV-PDs) have received great attention. Compared to conventional photoconductors, PEC UV-PDs exhibit a number of merits, including low cost, environmental friendly, self-powered, and fast response. This tutorial review provides a comprehensive introduction to this research field, covering from the basics of performance evaluation for PEC UV-PDs, the state-of-the-art progresses in structure designs, electrolyte matching, and electrode fabrications of PEC UV-PDs, to the integration of multiple functions into a PEC UV-PD. In the end, we present our perspectives on the future development of PEC UV-PDs and highlight the key technical challenges aiming to stimulate further developments in this research field.

KEYWORDS:

Ultraviolet photodetectors; Photoelectrochemical; Self-powered; Photoanode designs; Nanostructures;

1 Introduction

As well known, ultraviolet (UV) light is a "double-edged sword", can bring not only benefits to our daily lives, but also harms. And, it is very important for us to precisely measure and control UV irradiation. Due to their simple device structure and high On/Off ratios, UV photodetectors (UV-PDs) based on photoconductance were considered to be very promising for practical applications.[1-4] Their working principle is based on the conductance change of the semiconductors under illumination, namely photoconductivity (Fig. 1a).[5, 6] It can be understood that, in a semiconductor, electron-hole pairs are generated when illuminated by the photons that possess energy larger than its band gap. The generated holes are usually trapped at the surface, and the electrons transit to the conduction band (CB) and become quasi-free, resulting in an increase in the conductivity. So far, a number of wide-band-gap semiconductors (such as ZnO,[7] TiO_2,[8] SnO_2,[9] ZnS,[10] etc.) have been used for photoconductive UV-PDs, and various nanostructures (nanoparticles (NPs), nanowires (NWs), nanotubes (NTs), and nanotube/nanowire arrays (NTAs/NWAs)) and/or nano-composites have also been adopted to improve their performances.[11]

Generally, the performances of a photoconductive PD involve two aspects, namely the absorption of the incident light and the separation/transport of photogenerated electrons.[12-14] The magnitude of the conductivity change depends upon the quantum yield of carrier generation and the mobility of photogenerated carriers. As schematically illuminated in Fig. 1b-c, the photo detecting process is normally determined by the absorption and desorption of oxygen molecules in air,

both of which are slow processes that leading to a low photoresponse.[15-19] Moreover, this type of UV-PDs usually needs an external power source, which will limit their potential applications in the harsh environment.

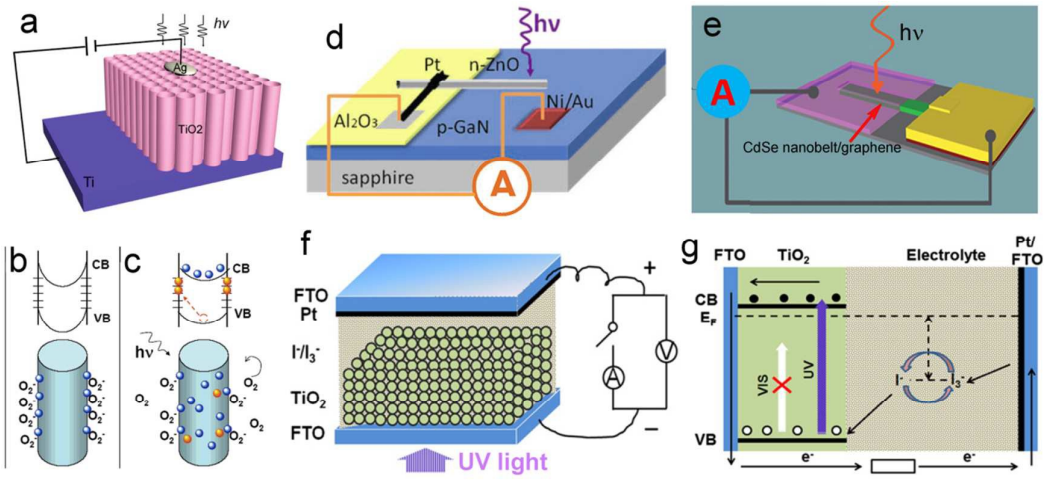

Fig. 1 (a) Schematic of a conventional photoconductor based on TiO_2 nanotube arrays (TNTAs). (b-c) Trapping and photoconduction mechanism in TiO_2 NWs. (d) Schematic of ZnO-GaN p-n junction. (e) CdSe/graphene Schottky junction UV-PDs. (f) Schematic of self-powered UV-PD based on PEC cells, and (g) working mechanism of the PEC UV-PD. (a) and (b-c) Reproduced from ref. 6 and 7, respectively. Copyright© 2010 and 2007 American Chemical Society. (d) Reproduced from ref. 20. Copyright© 2011 Wiley-VCH. (e) Reproduced from ref. 21. Copyright© The Royal Society of Chemistry 2012. (f) Reproduced from ref. 22. Copyright© 2012 Elsevier Ltd.

To solve the aforementioned problems, Schottky and p-n junctions are introduced into self-powered UV-PDs, which in nature are optoelectronic conversion devices similar to solar cells. The self-powered UV-PDs based on p-n junctions are constructed using a pair of p- and n-type semiconductors with wide-band-gap, forming a p-n junction photodiode (Fig. 1d).[23, 24] This type of photodiodes can convert the incident light into electrical signal without the necessity of external power. Furthermore, the photodiode usually possesses a good spectral selection (visible-blind) and fast photoresponse (rise time (t_r) of several ten μs, decay time (t_d) of several hundred μs). As illuminated in Fig. 1e, a UV-PD based on Schottky junction is

constructed using a metal/semiconductor interface, in which the semiconductor possesses a wide-band-gap. When illuminated by UV light (photon energy is larger than the E_g of the used semiconductor), the electron-hole pairs are generated and quickly separated due to the built-in electric field induced by Schottky junctions, showing a photovoltaic (PV) effect. Schottky-junction PDs often show extremely high photosensitivity (ratio of $(I_{photo}-I_{dark})/I_{dark}$) and fast photoresponse (less than 100 μs).[25, 26] Although many achievements have been obtained, especially ultra-fast photoresponse and extremely high photosensitivity, the reported self-powered PDs based on p-n or Schottky junctions usually show low spectral responsivity and high cost (complex fabrication process), limiting their real applications.[27]

Recently, photoelectrochemical (PEC) self-powered UV-PDs have attracted great attention.[22] As shown in Fig. 1f, this type of UV-PDs possesses a similar device configuration to other PEC devices, which, in principle, is a PEC PV device. Fig. 1g shows the working mechanism of the PEC UV-PDs using wide-band-gap semiconductor as photoanode. When the nanocrystalline TiO_2 (nc-TiO_2) film is illuminated by UV light, the absorbed photons will promote electrons from the valence band (VB) to CB, e_{CB}, leaving behind a hole, T^+,

$$T + h\nu \rightarrow T^+ + e_{CB}.$$

The photogenerated holes then migrate to the semiconductor/electrolyte interface and trap an electron donor in electrolyte (D), leaving the oxidized redox species, D^+,

$$T^+ + D \rightarrow T + D^+,$$

while the e_{CB} will diffuse through the nc-TiO_2 film and reach the transparent

conductive oxide (TCO) electrode, becoming external circuit electrons (*e*). On the other hand, the formed D^+ will diffuse through the electrolyte and reach the counter electrode. Then, the D^+ will be reduced by the *e* at the counter electrode, completing the circuit.

$$D^+ + e \rightarrow D \, .$$

Therefore, in this type of PEC UV-PDs, light harvesting and photogenerated carrier transport are achieved simultaneously.

Compare to the reported self-powered photoconductors based on p-n junctions and/or Schottky junctions, PEC UV-PDs usually exhibit two advantages:[28-34] 1) much higher photo responsivity. Most of the reported p-n junctions and/or Schottky junctions are made up of semiconductor nanoscale units, which usually lead to current output signals of nA order and require high-precision galvanometers; while the PEC UV-PDs can output large current of μA order. 2) Simple fabrication process and low cost: the fabrications of p-n junctions and/or Schottky junctions usually require not only complex process, but also high-purity semiconductor raw materials, both of which determine their high cost; while the PEC UV-PDs are usually fabricated via a physicochemical route, which shows low requirements in fabrication and cost. Nevertheless, this proposal of PEC UV-PDs might open a new insight for the development of cheap, easy-fabricated, self-powered UV-PDs with high spectral responsivity, high photo sensitivity and fast photoresponse.

The aim of this review is to sum up the recent advances in PEC self-powered UV-PDs, including 1) the basics of performance evaluation of PEC UV-PDs for easy

understanding of different research approaches and diverse performance metrics reported in the literatures; 2) the latest developments in electrolyte and photoanode designs for PEC UV-PDs, involved various electrolytes, various wide-band-gap semiconductors, various micro-/nano-scale morphologies/modifications/hybrids; and further analyze their effects on the properties of photoanodes (such as power conversion efficiency (η), photocurrent density (J), spectral responsivity, and photosensitivity). In this context, we provide examples from recent experimental results to elucidate these concepts in this section. And we will finally give an outlook on future directions in the research of PEC UV-PDs aiming to excite more research interest and stimulate further research progress in this research field.

2 Performance evaluations of PEC UV-PDs

The basic performance metrics for a PEC self-powered UV-PD usually include spectral responsivity, photosensitivity, response time, incident photo-to-current conversion efficiency (IPCE), etc.[28, 31-36] These parameters indicate how a detector responds and are described as follows:

Spectral responsivity (R_λ, A W^{-1}) is the ratio of photocurrent (I_p) to incident light power. It mainly depends on wavelength of incident UV light. The plot of responsivity as a function of wavelength gives the spectral response of a PD. The R_λ can be evaluated by,

$$R_\lambda = \frac{I_p}{P_{inc}} = \frac{\eta q}{h\nu},$$

where P_{inc} is the incident optical power in watts, h is the Plank constant, ν is the light frequency, q is the electron charge, and η is the ratio of photogenerated electron and

incident photon numbers.

Photosensitivity (S), or named as ON-OFF ratio, is the ratio between I_p and dark current (I_d), i.e.,

$$S = \frac{I_p - I_d}{I_d} \times 100\% .$$

This ratio depends on both I_p and I_d, reflecting not only the optoelectronic conversion performances of the devices, but also the transport characteristics of electrons in the devices' photoanodes.

Response time (t): is used to characterize the speed of response to a sudden change in the input signals, i.e., to measure the time required for a PD's response to a light pulse. The response time is specified as the time taken for the photocurrent rising or decaying to a specific value under "ON" or "OFF" state of light illumination. The t_r is often defined as the time that photocurrent increases from 0 to 63% (i.e., 1-1/e) of the maximum value, and the t_d is the time that photocurrent decreases from the maximum value to 37% (i.e., 1/e).

In most cases of PEC UV-PDs, the response speed is limited by the t_d, rather than the t_r, which is quite different to other types of UV-PDs.[37] In fact, the t_r of a PEC UV-PD is mainly dependent on two fundamental aspects: (1) the time of the e_{CB} generated on the solid/liquid interface diffusing to the TCO electrode via the wide-band-gap semiconductor films; (2) the time of the D^+ drifting to the counter electrode via the electrolyte. The drift process of D^+ through the electrolyte is usually quite rapid due to free ion transport in the electrolyte, while the e_{CB} diffusion process is greatly influenced by the recombination time and is relatively slow. The diffusion

time can be improved by ensuring that all electron–hole pairs be separated and transported through the electrode films under built-in electric field of the semiconductor junctions.

IPCE: is defined as the ratio of output I_p (electrons per second) to incident photon fluence (photons per second) on the device. It mainly depends on light harvesting efficiency (LHE (λ)), electron injection efficiency (ϕ_{inj}), and electron collection efficiency (η_c). Then IPCE can be roughly expressed by,[38]

$$\mathrm{IPCE}(\lambda) = \mathrm{LHE}(\lambda) \times \phi_{inj} \times \eta_c .$$

Thus, what we can do to increase IPCE value is to improve LHE(λ), ϕ_{inj} and η_c, which generally guide the potential research directions in PEC fields. On the other hand, using R_λ, IPCE can be also estimated using,

$$IPCE = R_\lambda \times E_{ph} = \frac{I_p}{P_{inc}} \times E_{ph} = \frac{h\nu}{qP_{inc}} I_p ,$$

where E_{ph} is the photon energy measured in eV. As for certain incident UV light, the IPCE value is in direct proportion to the output I_p. This is to say that IPCE and I_p are equal for quantitative UV detecting.

Some important issues should be noted here for graduate students or researchers who are new in the research of PEC UV-PDs. First, the methodologies to reliably choose and prepare a material for use as an PEC UV-PD electrode are not well standardized due to the reported different techniques and parameters (e.g. different device structures (three-electrode or two-electrode), different calculations of response time (0 to 1-1/e, 0 to 90%, or 0 to stable value), different electrode kinds/materials/morphologies, different electrolytes/ions, different UV light

wavelengths), thus yielding widely varying results. Second, the requirements in electrode materials are not the same with those to dye sensitized solar cells (DSSCs) or photocatalytic cells; e.g., IPCE value is not the first important parameter for PEC UV-PDs. Third, for a high-performance UV-PD, it should be "visible-blind" for high UV selection, and "linear output" for quantitative UV measuring. This is to say, these two aspects are also important performance metrics for UV-PDs.

Overall, various performance metrics discussed above indicate that the UV detecting performances of the PEC devices are mainly determined by the photoanodes. Current research efforts are focused on improving optoelectronic performance of the frequently-used photoanode materials (such as ZnO, TiO_2 and SnO_2), including spectral responsivity, photosensitivity, response time, visible-blind and linear-output characteristics. In addition, the used electrolytes and multi-functional PEC UV-PDs are also simply reviewed, as well as the preparation of micro-/nano-structure of photoanodes. And the recent results are summarized in Table 1.

Table 1. Photoresponse performances of PEC UV-PDs based on various nanostructures of ZnO, TiO_2, and SnO_2

Nanostructures	Conditions	Electrolyte type	Electrode system	J_p ($\mu A\ cm^{-2}$)	S $((I_P-I_d)/I_d)$	t_r (s)	t_d (s)	Estimate method of t	R_λ ($mA\ W^{-1}$)	Visible blind	Linear output	Refs.
hydrothermal ZnO NRs	250-600 nm, 100 mW cm^{-2}, 0 V	0.1 M Na_2SO_4	3-electrode	1.5	7	4.9	134.3	Biexponential function fitting	-	No	-	39
ZnO(N) NR films	390 nm, 3 mW cm^{-2}	Spiro-MeOTAD	2-electrode	50	300	4×10^{-3}	1×10^{-2}	10% to 90%	17 at 390 nm	Yes	-	40
TiO_2 NRAs	365 nm, 0.7 mW cm^{-2}	poly(9,9-dihexylfluorene)	2-electrode	1.78×10^{-2}	1000	< 0.2	< 0.2	Estimated by the test limit	33 at 395 nm	Yes	-	41
ZnO nanoneedles	365 nm, 1.25 mW cm^{-2}	DI water	2-electrode	4.1	-	0.1	0.1	10% to 90%	22 at 385 nm	Yes	no	30
TiO_2@ ZnO nanostrawberries	365 nm, 20 mW cm^{-2}	I^-/I_3^-	2-electrode	379	37899	0.022	0.009	0 ~ 1, 1 ~ e^{-1}	17.85 at 365 nm	Yes	yes	29
ZnS/ZnO NRAs	Xe lamp, 100 mW cm^{-2}, 0 V	0.5 M Na_2SO_4	3-electrode	50	-	-	-	-	-	Yes	-	42
TiO_2 films by ALD	365 nm, 2.44 mW cm^{-2}	water	2-electrode	100	10^6	< 0.5	< 0.5	0 to 1	69 at 350 nm	Yes	yes	43
nc-TiO_2 films	365 nm, 33 mW cm^{-2}	I^-/I_3^-	2-electrode	550	2698	0.08	0.03	0 ~ 1, 1 ~ e^{-1}	16.7 at 365 nm	Yes	yes	22
TiO_2 NRAs	365 nm, 3 mW cm^{-2}, 0 V	0.5 M Na_2SO_4	3-electrode	15	6	< 0.1	< 0.1	-	5 at 365 nm	-	no	44
TiO_2 NRAs	365 nm, 10 mW cm^{-2}	DI water	2-electrode	40	-	0.15	0.05	0 ~ 90%, 1 ~ e^{-1}	25 at 350 nm	Yes	-	36
TiO_2 NRAs	365 nm, 2.5 mW cm^{-2}	liquid crystal- I^-/I_3^- gel	2-electrode	175	-	< 0.03	< 0.03	0 ~ 90%, 1 ~ e^{-1}	90 at 383 nm	Yes	yes	33
TiO_2 nano-branched arrays	365 nm, 2 mW cm^{-2}	I^-/I_3^-	2-electrode	373	-	0.15	0.05	0 ~ 90%, 1 ~ e^{-1}	220 at 352 nm	Yes	-	34
Dendriform TiO_2 NWs	365 nm, 25 mW cm^{-2}	I^-/I_3^-	2-electrode	570	1902	0.0053	0.0059	0 ~ 1-e^{-1}, 1 ~ e^{-1}	22.8 at 365 nm	Yes	yes	45
TNRCs	254/365 nm, 1.55 mW cm^{-2}, 0 V	I^-/I_3^-	2-electrode	17	-	1.7	2.1	0 to 1	19 at 345 nm	Yes	yes	35
TNRs				235	-	0.3	0.1		89 at 355 nm	Yes	yes	
Multilayer TNRC/TNRs				278	-	0.3	0.2		152 at 360 nm	Yes	yes	
TNTAs	250–385 nm, 0 V	0.1 M NaOH	3-electrode	210	-	< 0.2	< 0.2	0 ~ 1	11.2 at 350 nm	Yes	-	46
$SrTiO_3$–TiO_2 heterojunction				650	-	< 0.2	< 0.2		18.6 at 350 nm	Yes	-	
B-SnO_2 NFs	365 nm, 40 mW cm^{-2}	I^-/I_3^-	2-electrode	900	4549	0.03	0.01	0 ~ 1, 1 ~ e^{-1}	22.5 at 365 nm	Yes	yes	28
SnO_2@TiO_2 microtubes	365 nm, 1.55 mW cm^{-2}	I^-/I_3^-	2-electrode	100	-	< 0.1	< 0.2	0 to 1	~ 52 at 340 nm	Yes	-	32
SnO_2 microtubes				78	-	< 0.1	< 0.2		~ 38 at 340 nm	Yes	-	
TiO_2- SnO_2 hollow nanospheres	365 nm, 35 mW cm^{-2}	I^-/I_3^-	2-electrode	1277	4020	0.03	0.01	0 ~ 90%, 1 ~ e^{-1}	36.48 at 365 nm	Yes	yes	31
B-TiO_2 nanoneedles-SnO_2 nanosheets	365 nm, 40 mWcm^{-2}	I^-/I_3^-	2-electrode	709.5	4404	0.02	0.004	0 ~ 1, 1 ~ e^{-1}	17.7 at 365 nm	Yes	yes	47

3 Recent developments in PEC UV-PDs

3.1 Prototype for PEC self-powered UV-PDs

PEC UV-PDs possess a similar device configuration to other PEC devices, evolved from a photoanode/electrolyte/counter electrode sandwich structure. Thus their working mechanisms are to some extent the same with that of other PEC devices. Generally, the improvement in detecting performances of PEC UV-PDs hinges on the development of the combination of electrolyte (redox couples), counter electrode, and photoanodes.[48] In 2011, Lee *et al*. first reported a type of UV-PDs based on a TiO_2/water solid-liquid heterojunction,[43] containing two electrodes of 50-nm TiO_2/Fluorine-doped Tin Oxide (FTO) electrode and 50-nm Pt/indium tin oxide (ITO). Both electrodes were assembled together using a sealant and some water used as an electrolyte was poured into the space between them. Under UV illumination (365 nm, 0.244 μW cm^{-2} to 0.113 mW cm^{-2}), the I_p of the devices linearly increases with increasing incident light power, exhibiting excellent reproducible photoresponse with fast response speed (both decay and rise time are less than 0.5 s). Here, it is noted that this linear variation of I_p will make this type of UV-PDs be easily used for quantitative measurement of UV light. Moreover, the S can reach an order of magnitude of 6 under 479-μW UV illumination, and the devices show a visible-blind characteristic, exhibiting their maximum responsivity of ~ 69.2 mA W^{-1} at ~ 350 nm. Thus, it can be seen that this type of UV-PDs possesses an exceptional competence for UV light detecting and presents a promising direction for future development of commercially low-cost UV-PDs.

Alternatively, three-electrode configuration is also adopted to test the electrochemical performances of electrode materials. For instance, Majumder *et al*.[39] tested the PV response of hydrothermal ZnO nanorod arrays (ZnO NRAs) grown on FTO substrate using a three-electrode system, in which Ag/AgCl served as the reference electrode, Pt wire as

counter electrode, and 0.1 M Na_2SO_4 aqueous solution as electrolyte. The ZnO NRAs show stable and repeatable PV response, showing a quick increase in PV but a slow recovery. And, the ZnO NRAs show the maximum PV at 350 nm and good visible-blind characteristics. In strict sense, this three-electrode configuration is not a real device. However, it is technically more challenging to precisely analyze and discuss on limited results from the reported two-electrode PEC cells. So, to get a far and wide discussion on PEC UV-PDs, the results from three-electrode system have also been put into the whole frame for comparison.

3.2 PEC UV-PDs based on various electrolytes

The electrolyte is one of the most crucial components that provide pure ionic conductivity between the photoanode and counter electrode in PEC UV-PDs.[49] Redox electrolytes in UV-PDs can not only function as the medium for the inner carrier transport between electrodes, but also continuously reactivate the semiconductor and itself during the operation. Thus, several aspects are essential for the electrolytes used in PEC UV-PDs: 1) The electrolytes must be able to transport the carriers between photoanode and counter electrode. Once the electrons are promoted from the VB to CB, the remaining holes will be rapidly oxidized by electron donors in electrolyte. 2) The electrolytes must guarantee fast drift of carriers (higher conductivity) and show large interfacial contact with the mesoporous semiconductor photoanode and the counter electrode. 3) The electrolyte should be chemically stable and inert to photoanode materials, which guarantees the efficiency and long-term stability of the PEC devices. According to physical states, compositions, and formation mechanisms, the electrolytes used in PEC UV-PDs can be broadly classified into: aqueous electrolyte, organic liquid electrolyte, or quasi-solid gel electrolyte. Xie's and Shen's groups reported PEC self-powered UV-PDs assembled using the traditional liquid I^-/I_3^- redox couple electrolyte.[22, 28, 29, 31, 32, 35, 45, 47] And impressive performances were observed in these UV-PDs. However, liquid I^-/I_3^- redox couple electrolyte is not ideal for long-term operation, because it

is highly corrosive, volatile, and photo-reactive, which often make it interact with common metallic components and sealing materials.

Aqueous electrolytes are more suitable for PEC self-powered UV PDs due to that water is one of the safest, most stable, and most environment-friendly electrolyte. And a type of UV-PD based on TiO_2/water solid–liquid heterojunction has been proposed recently.[30, 36, 43] Interestingly, this TiO_2/water-based UV-PD can exhibit high photosensitivity, excellent spectral selectivity, linear variations in I_p, and fast response.[43] Moreover, Chen's group reported that TiO_2 NR/water-based self-powered UV-PDs showed a spectral responsivity of 25 mA W^{-1} and a fast photoresponse.[36] Furthermore, many aqueous electrolytes have been used during PEC tests, such as Na_2SO_4,[39, 42, 44, 50-57] and KOH.[58-60] Cao *et al*. reported the I_p response of TiO_2 nanorod arrays (NRAs) under UV illumination using 0.5 M Na_2SO_4 aqueous electrolyte,[44] in which TiO_2 nanostructures can harvest more incident light photons compared to a flat thin-film active layer because of the markedly enlarged TiO_2/electrolyte contact area. The photocurrent density (J_p) can reach 12.87 μA cm^{-2} under UV illumination (365 nm, 3 mW cm^{-2}). Though aqueous electrolytes are safe, stable, and environment-friendly, the performances of these UV-PDs are poorer compared those with I^-/I_3^- electrolyte. So, further more research is required for the development on the aqueous electrolyte.

Using aqueous electrolytes as the medium for the carrier transport, great developments have been achieved in various PEC devices. However, liquid electrolytes often causes some practical problems, such as leakage, volatilization of solvent, corrosion of counter electrode, and ineffective sealing of the cells for long-term applications. Recently, a type of quasi-solid-state electrolyte has been used in PEC cells. Han *et al*. demonstrate a high spectrum selectivity from TiO_2-NRA-based UV-PDs by using poly(9,9-dihexylfluorene) as the electrolyte.[41] The maximum response of 33.2 mA W^{-1} at 395 nm is obtained under zero

bias. However, the J_p is only about 1.78 $\times 10^{-5}$ μA cm^{-2} under 0.7-mW-cm^{-2} 365-nm UV illumination. More recently, Chen's group reported a nanostructured quasi-solid-state UV-PDs fabricated using a liquid crystal (LC)-embedded I^-/I_3^- electrolyte with a light-trapping scheme.[33] The maximum responsivity is about 90 mA W^{-1} at 383 nm; the maximum IPCE is about 29%. Under 2.5 mW cm^{-2} UV illumination (365 nm, 0 V), the J_p reaches 175 μA cm^{-2} with t_r less than 0.03 s. Moreover, Game *et al*. report a facile solution-processed fabrication of a self-powered organic-inorganic hybrid PD using n-type oriented ZnO NRs and p-type Spiro-MeOTAD semiconductor.[40] The assembled UV-PDs show a high S (10^2), a high UV/visible ratio (300) and a fast photoresponse (t_r of 200 μs and t_d of 950 μs). Under UV illumination (390 nm, 3 mW cm^{-2}), a J_p of 50 μA cm^{-2} can be obtained. Although the efficiencies of these UV-PDs with quasi-solid-state electrolytes are often lower than those of the UV-PDs with liquid electrolytes, the quasi-solid electrolytes may become viable alternatives to the liquid electrolytes owing to the greatly improved stability and sealing ability, which will be beneficial to their practical applications.

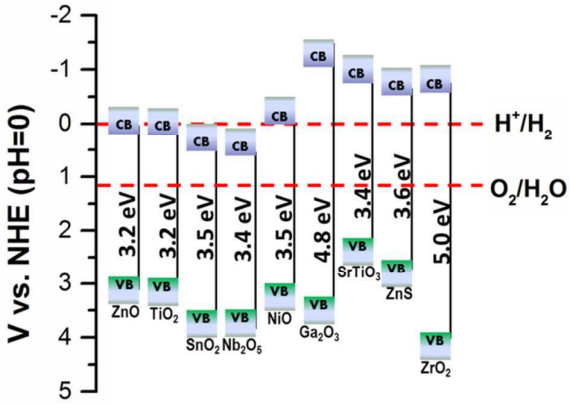

Fig. 2 Schematic diagrams illustrating the energy levels of the CB and VB of various wide-band-gap semiconductors.

3.3 PEC self-powered UV-PDs based on various photoanodes

So far, most work to enhance the performances of PEC UV-PDs has been focused on developing photoanodes with high photoresponse, including spectral responsivity, photosensitivity, and response time. The key findings can be reviewed from Table 1.

Researchers have used different materials, micro-/nano-structures, electrolytes, counter electrodes, and even diverse device structures to report the UV detecting performances of the assembled PDs, which make it difficult to directly compare some results in the literatures. In general, short-circuit photocurrent (I_{sc}) or density (J_{sc}) of electrode materials is obtained using either the assembled two-electrode cell or three-electrode system. Moreover, many studies have reported the "visible-blind" and "linear output" characteristics, even though the estimate methods of photosensitivity, ON-OFF ratio, rise and decay time are not always consistent. Thus, we have marked the different methods used in Table 1 for easy comparison. And it can be seen that various nanostructures were exploited for constructing photoelectrodes in PEC cells, including NPs, NRs, NWs, NTs, NRAs, nanosheets (NSs), and nano-forests.[61] It is suggested that the electron transport rates of these nanostructures above is in the sequence of NP films < NR films < nano-forest films < NRA films, while the sequence for specific surface area (SSA) turns out to be NP films > NR/NW films > nano-forest films > NTA films > NRA/NWA films. Thus, there need a strategy to balance the choice for constructing PEC electrodes.

On the other hand, the band-gap energy of photoanode for UV-detecting should be larger than 3.1 eV, corresponding to the wavelength of 400 nm. The recently reported wide-band gap oxide nanostructures (including binary metal oxides like ZnO (ZnS),[42] TiO_2,[11] SnO_2,[62] NiO,[63] Nb_2O_5,[64] Ga_2O_3,[65] ZrO_2,[66] and ternary metal oxide like $SrTiO_3$[64]) can be potentially applied as photoanode materials for PEC UV-PDs (Fig. 2). So far, ZnO, TiO_2 and SnO_2 are the most frequently studied materials for PEC cells, and in this context, we present them in three sub-sections, i.e. ZnO, TiO_2, and SnO_2 nanostructured photoanodes.

3.3.1 TiO_2 nanostructures for PEC UV-PDs

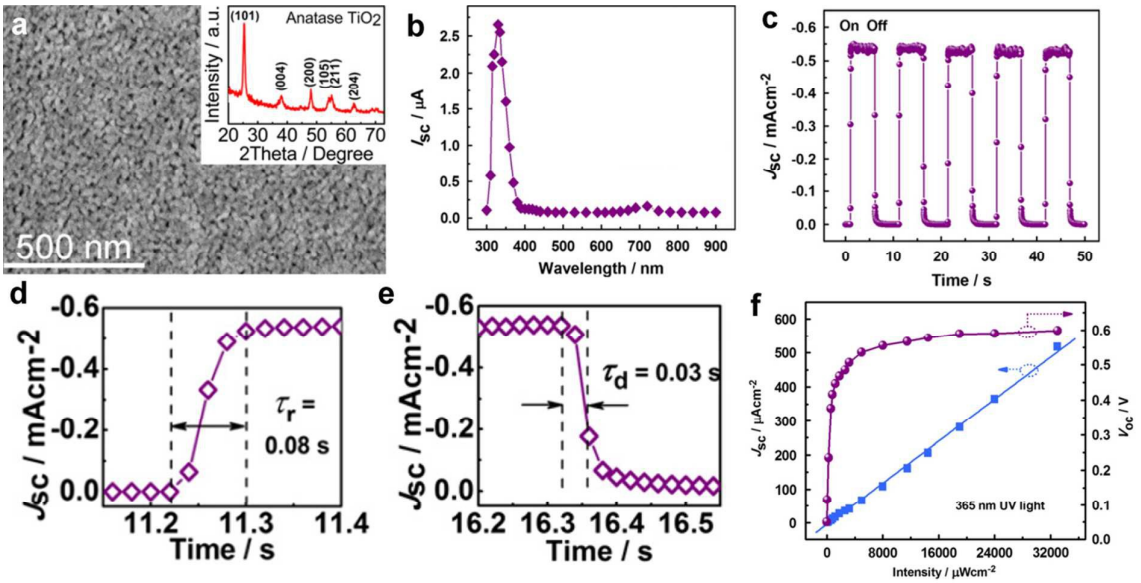

Fig. 3 (a) SEM image of the spin-coated TiO_2 films, and the inset is the corresponding XRD spectrum; (b) spectral responsivity of the self-powered UV-PDs, indicating a visible-blind characteristic; (c) time responses of J_{sc} under UV illumination (365nm, 33 mW cm^{-2}) measured for light-on/off states; (d-e) enlarged rise and recovery edges of the current response under light intensity of 33 mW cm^{-2}, respectively; (f) J_{sc} and V_{oc} as a function of the incident UV (365 nm) intensity. Reproduced from ref. 22. Copyright© 2010 Elsevier Ltd.

TiO_2 is n-type semiconductor with a wide band-gap (anatase 3.2 eV and rutile 3.0 eV) and has been frequently studied for UV detecting due to its distinctive UV absorption characteristics.[67, 68] TiO_2 NP, NR, NT, and nano-forest films have been employed in the photoanodes for PEC UV-PDs. [22, 34, 36, 44, 45, 59] In 2012, Xie's group first formally proposed a prototype for PEC UV-PDs, as shown in Fig. 1e-f.[22] The nc-TiO_2 films were used as photoanodes, which were prepared by the traditional sol-gel method and spin-coated on FTO glass. The resultant anatase TiO_2 nanoparticles possess an average diameter of ~17 nm (Fig. 3a), and the optimized film thickness is ~ 450 nm for 365-nm UV light in this case. Then, a dried TiO_2 photoanode and a platinized counter electrode were assembled into a sandwich cell, and the traditional I^-/I_3^- ionic liquid was used as the electrolyte. The assembled devices show the highest I_p response at ~330 nm (Fig. 3b), accompanying a good UV selectivity and a visible-blind property, which is very important to a UV-PD. Under UV illumination (365 nm, 33 mW cm^{-2}), the J_{sc} signal is reproducible under "ON" or "OFF" state of UV light, and reaches 550 μA cm^{-2} with R_λ of 16.7 mA W^{-1} (Fig. 3c). Moreover, the S of the PDs is found to

be about 269.8, and the t_r and t_d are ~ 0.08 and 0.03 s for J_{sc} signals, respectively (Fig. 3d-e). These results suggest that these assembled cells possess a high photosensitivity to UV light (365 nm). And the J_{sc} increases linearly with increasing the UV light intensity in a wide variation range from 25 μW cm^{-2} to 33 mW cm^{-2} (Fig. 3f), which might benefit their real application in quantitative measurement for UV light. However, the value of R_λ and S is not as high as the published results.[43] Nevertheless, this work successfully started up a new research area of PEC UV-PDs.

Another suitable nanostructure of TiO_2 for UV-PDs is vertical NRAs due to their relatively high transport rates of electrons and enhanced transfer of electrolyte ions because of more interfaces between the NRs and the solution compared to a flat thin-film active layer. It is demonstrated that the basic parameters of NRAs (such as diameter, length and density) greatly affect the performances of PEC cells. Cao *et al*.[44] found that under UV illumination (365 nm, 3 mW cm^{-2}, 0.5 M Na_2SO_4, three-electrode system), 3-μm-long TiO_2 NRAs show a J_p of about 15 μA cm^{-2}, while 6-μm-long TiO_2 NRAs only 6 μA cm^{-2}, suggesting that suitable length of NRAs is required for a high J_p. In view of this point, Chen's group applied vertical rutile TiO_2 NRAs (~ 1 μm in height, 100 to 150 nm in diameter, 20 NRs μm^{-2} in density) into PEC UV-PDs (Fig. 4a-b).[36] Under UV illumination (365 nm, 1.25 mW cm^{-2}, DI water), the J_p is 4.67 μA cm^{-2} with R_λ of 4 mA W^{-1}. This low responsivity should be mainly attributed to the high resistance of the used water electrolyte. Meanwhile, this device show a fast photoresponse, i.e., the t_r of 0.15 s and the t_d of 0.05s, indicating a rapid photoresponse characteristic. Moreover, the maximum responsivity of the photoanodes reaches about 25 mA W^{-1} at 350 nm.

Compared to NRAs, TiO_2 NTAs (TNTAs) are also attractive in the field of PEC applications, such as DSSCs, photocatalyst, and UV-PDs, due to their enlarged TiO_2/electrolyte interface and well-defined carrier transport path, most importantly, ease of

fabrication and low cost. [6, 69] Li *et al.*[59] reported that under UV illumination (365±15 nm, 70 mW cm^{-2}, 0 V bias), the 3-μm-long TNTAs exhibit a J_p of ~100 μA cm^{-2} with R_λ of 1.4 mA W^{-1}. And the J_p can also quickly drop to zero when switching off the light source, indicating fast charge transport in NTAs. However, compared to the nc-TiO_2, both TiO_2 NRA and NTA films show a much lower R_λ, which may be due to their lower SSA and thus lower light harvesting efficiency.

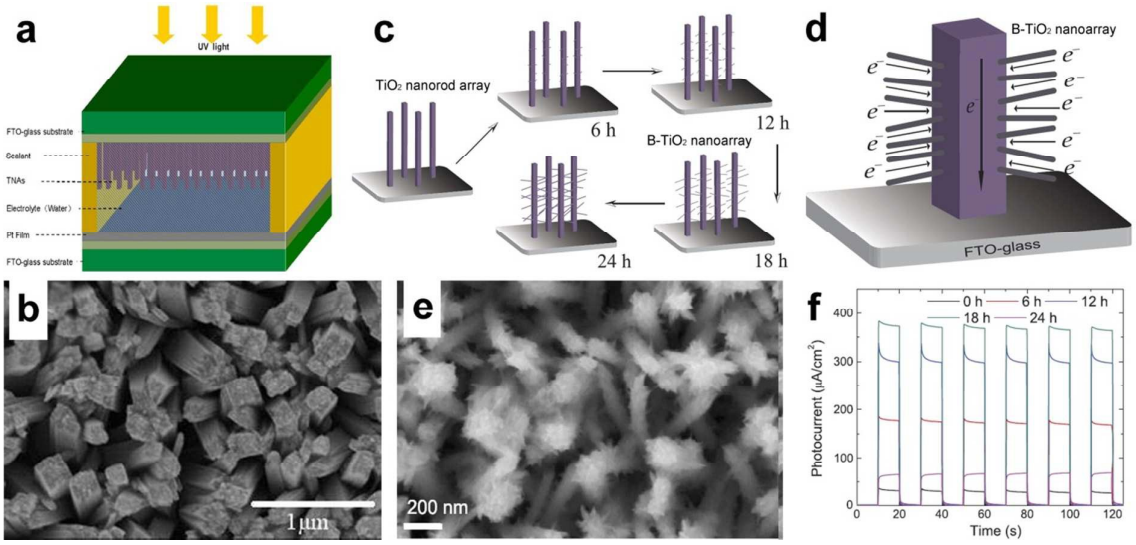

Fig. 4 (a) Schematic device structure of the PEC UV-PDs using water as electrolyte, and (b) top-view SEM image of TiO_2 NRAs. (c) Schematic formation process of B-TiO_2 NRAs grown on FTO glass, (d) scheme of the possible electron transport mechanism in a B-TiO_2 NRA photoanode, (e) top-view SEM image of B-TiO_2-18h NRAs, and (f) time responses of J_ps for different PDs under UV light pulsed illumination (365 nm, 2 mW cm^{-2}). (a-b) Reproduced from ref. 36. Copyright© 2013 Springer. (c-f) Reproduced from ref. 34. Copyright© 2014 IOP Publishing.

It is reported that branched TiO_2 (B-TiO_2) nanostructures (i.e., nano-forest) usually possess better charge transport and light absorption properties than NP films, and larger SSAs than NRAs/NTAs.[70-72] Chen's group prepared B-TiO_2 NRAs by a facile two-step chemical synthesis process and assembled them into photoanodes (Fig. 4c-d).[34] Under UV illumination (365 nm, 2 mW cm^{-2}), the assebled PEC UV-PDs (18 h, Fig. 4e-f) also exhibit a high J_p of 373 μA cm^{-2} with R_λ of 186.5 mA W^{-1}, which is greatly enhanced compared to those of the above single-phase TiO_2 NRA/NTA and nc-TiO_2 films. Moreover, the UV-PDs also show a fast photoresponse (t_r of 0.15 s and t_d of 0.05 s). These improved performances are attributed

to markedly enlarged TiO_2/electrolyte contact area and high electron conductivity in TiO_2 NR trunk. However, it can be seen that the enhanced light scattering by B-TiO_2 NRAs leads to lower transmission in visible light region, which is harmful to spectral selectivity of a UV-PD.

3.3.2 ZnO nanostructures for PEC UV-PDs

Due to its easy fabrication, low cost, and unique physical/chemical properties, ZnO is applied as building units in many optoelectronic devices, such as solar cells, nanogenerators, and field effect transistors.[61, 73] Recently, the application of ZnO in UV light detecting has attracted much interest because of its wide band-gap (3.37 eV) and high electron mobility (200 $cm^2\ V^{-1}\ s^{-1}$).[67, 74] It has been demonstrated that rationally designed ZnO nanostructures with complex shape and compositions can become one of the most promising building blocks as detectors for UVA range.[4] NP films were first used in various optoelectronic devices. Although NP films possess the highest SSA among various types of nanostructures, their high recombination losses and long transport distance of photogenerated carriers greatly reduce their optoelectronic performances.[75] It was found that under UV illumination (365 nm, 5 mW cm^{-2}) using 0.5 M Na_2SO_4 solution as electrolyte and three-electrode system, the highly-crystalline ZnO films only exhibit a J_{sc} of ~ 60 μA cm^{-2} with R_λ of 12 mA W^{-1},[54] which is even lower than that of nc-TiO_2 films.[22]

ZnO NRAs/NWAs have also been frequently used in PEC cells, such as water splitting and PV systems, due to their good conduction of electrons and holes, nontoxicity, environmental friendliness, and controllable low-temperature synthesis.[76, 77] Compared to NP films, NRAs usually possess higher light absorbance efficiency and lower electron recombination. Recently, Chen's group reported a type of PEC UV-PDs using hydrothermal-grown ZnO nanoneedles as the active photoanode and DI water as the electrolyte (Fig. 5a).[30] The resultant ZnO nanoneedles possess average length of 2-3 μm and

diameter of 80-100 nm at the base (Fig. 5b). The maximum R_λ of ZnO nanoneedle arrays is ~22 mA W^{-1} at ~385 nm, showing good spectral selectivity in the UVA range. Under UV illumination (365 nm, 1.25 mW cm^{-2}), the J_P is 4.08 μA cm^{-2} with R_λ of 3.26 mA W^{-1}. And both t_r and t_d of the device are ~ 0.1 s for J_{sc}, which will make ZnO nanoneedles arrays potential application in UV-PDs. However, the photoresponse region is obviously broadened to over 450 nm because of the light scattering between nanoneedles. This is unfavorable to UV detecting. And, it is found that there exists a gradual saturation in J_p under higher UV illumination, which might be due to the poor carrier transport ability of water.

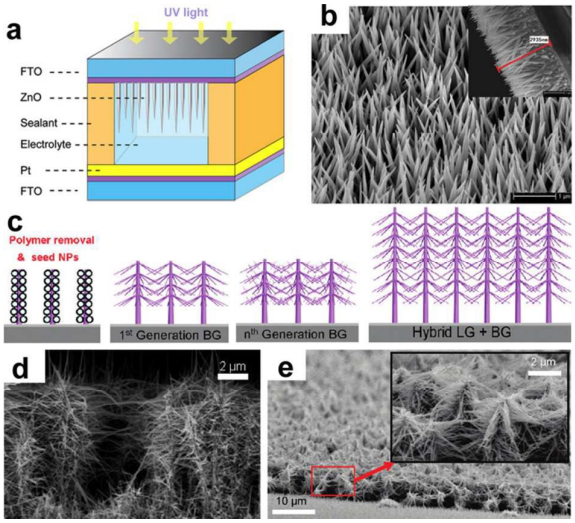

Fig. 5 (a) Schematic device structure of UV-PDs based on ZnO nanoneedle arrays and (b) SEM image of ZnO nanoneedle arrays, the inset shows their cross-sectional view. (c) Schematic growth route for ZnO NWAs with different branches, (d-e) SEM images of ZnO NWAs after one time branched growth and ZnO NW nano-forest, respectively. (a-b) Reproduced from ref. 30. Copyright© 2013 Springer. (c-e) Reproduced from ref. 78. Copyright© 2011 American Chemical Society.

Hierarchical branched nanostructures are another promising structure that provide a high light absorption for the optoelectronic devices.[79] Ko *et al.*[78] studied the effect of branched growth on the efficiency of hierarchical ZnO NWA photoanodes (Fig. 4c-e), and found that after one-time branched growth, the J_{sc} of 7 and 13-μm ZnO NWAs are significantly enhanced 389% and 256% compared to the pristine ones, respectively; while with one more branched growth, the J_{sc} of 13-μm ZnO NWAs can be further slightly enhanced ~14%. Thus, this J_{sc} increase can be explained by considering a combination of several effects:[80] i)

Enhanced light absorption from the enlarged SSA results in a large J_{sc} increase. ii) The dense network of crystalline ZnO NWs can increase the electron diffusion length and electron collection because the NWs provide direct conduction paths for electrons' transport from the injection points to the collection electrode. iii) Randomly branched NWs promote enhanced light-harvesting without sacrificing efficient electron transport. Furthermore, branched NWs also increase light-harvesting efficiency by scattering enhancement and trapping, which might be unfavorable to spectral selectivity of the assembled UV-PDs.

3.3.3 SnO_2 nanostructures for PEC UV-PDs

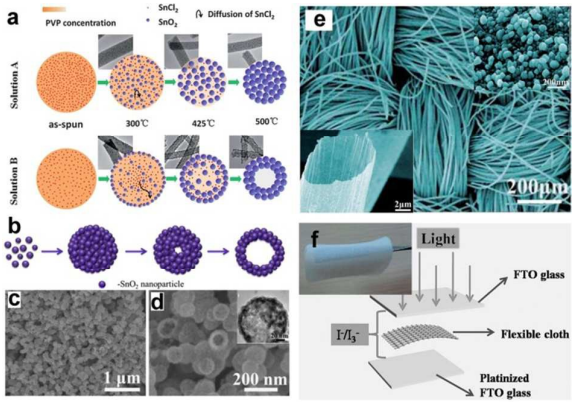

Fig. 6 (a) Schematic formation mechanism of SnO_2 NFs and NTs. (b) Schematic illustration of the formation of SnO_2 HNS, (c-d) SEM images of the prepared SnO_2 HNSs, inset in d is the TEM image. (e) Typical SEM images of SnO_2 cloth woven by microtubes, insets show amplified SEM images of a single SnO_2 microtube assembled by numerous NPs. (f) Structure scheme of the PEC UV-PDs, inset shows optical image of SnO_2 cloth. (a) and (e) Reproduced from ref. 81 and 82, respectively. Copyright© The Royal Society of Chemistry 2012 and 2013. (b-d) Reproduced from ref. 31. Copyright© 2014 Elsevier Ltd. (f) Reproduced from ref. 32. Copyright© 2014 Wiley-VCH.

Tin oxide (SnO_2) is an important n-type semiconductor with good sensitivities, including chemical sensing, bio-sensing and UV sensing properties.[9] Thus, SnO_2 has been considered to be another most promising alternative of TiO_2 for PEC UV-PDs due to its higher electronic mobility (~100-200 $cm^2 V^{-1} s^{-1}$) and larger band gap (3.6-3.8 eV) than TiO_2 (~0.1-1.0 $cm^2 V^{-1} s^{-1}$, 3.2 eV), fast response and "visible blind" characteristics together with excellent long-term stability. However, SnO_2-based PEC cells, including UV-PDs, were developed with less success, and the performances of SnO_2 photoelectrodes reported so far are much less than those of TiO_2. In view of this situation, Xie's group has conducted a series of studies on

enhancing the PEC performances of SnO_2 photoelectrodes using the traditional I^-/I_3^- electrolyte.[28, 31, 47, 81] First, SnO_2 nanofibers (NFs) were prepared using a mixture solution of polyvinylpyrrolidone (PVP) and $SnCl_2$ via an electrospinning technique.[28, 81] Under UV illumination (330 nm), the PEC UV-PDs based on SnO_2 NFs exhibit a J_{sc} of 15.8 μA cm^{-2}, which is far lower than that of nc-TiO_2 films (34.7 μA cm^{-2}). However, the SnO_2 NFs show a high J_d of 10.7 μA cm^{-2}, indicating a poor photodetecting performance. To further increase the SSA of electrospun SnO_2 NFs, SnO_2 NTs were designed combing a nanoscale Kirkendall effect (Fig. 6a).[83] Compared to SnO_2 NFs, The J_{sc} and η values of SnO_2-NT photoanodes are improved ~30% and 39%, respectively, which is yet far lower than those of P25.[81] On the other hand, the SnO_2 NSs directly grown on FTO glass were also applied into PEC UV-PDs.[47] Under UV light illumination (365 nm, 40 mW cm^{-2}), the UV-PDs show a J_{sc} of 30 μA cm^{-2} with R_λ of 0.75 mA W^{-1}, indicating a strong electron recombination at the interface between SnO_2 NSs and electrolyte. In view of this situation, Xie's group further assembled SnO_2 NSs into hollow nanospheres (HNSs) via a low-temperature synthesis (Fig. 6b-d),[31] and found that under UV irradiance at 330 nm, the SnO_2 HNS photoanodes show a much improved J_{sc} of 31.2 μA cm^{-2} with η of 3.3%, although which is yet far lower than that of nc-TiO_2 (40.8 μA cm^{-2} with η of 7.8%).

More recently, Shen's group has prepared a type of SnO_2 microtubes using carbon cloth as sacrificial templates,[32, 82] which can be directly used as a binder-free photoanode (Fig. 6f). These microtubes consist of rutile SnO_2 NPs with size of several tens of nanometers (Fig. 6e). The assembled PEC UV-PDs using I^-/I_3^- electrolyte show a high J_p response of 78 μA cm^{-2} with R_λ of 50.3 mA W^{-1} under UV illumination (365 nm, 1.55 mW cm^{-2}). Compared to TiO_2-based photoanodes, the poor performances observed from SnO_2 ones are mainly attributed to the fast interfacial electron recombination and lower trapping density.[84] Thus in latter session, we will give a review on recent work about the PEC performances of

SnO_2-based hybrid photoanodes, including: SnO_2 NF/NP, and SnO-TiO_2 hybrids.

3.4 Modification of photoanodes for high-performance UV-PDs

Similar to a optoelectronic cell, the strategies for enhancing performance of PEC PDs usually include three aspects, i.e., enhancing light harvesting in photoanodes (for high R_λ and S), and enhancing charge separation or reducing charge recombination (for repeatable and fast J_{sc} response), and enhancing charge transport (for short t_r and t_d). In this session, we will give a systematic introduction to these three strategies and detailed discusses on the designs of photoanodes for high-performance PEC UV-PDs.

3.4.1 Enhancing light harvesting efficiency

PEC UV-PDs are usually composed of an inorganic semiconducting photoanode, electrolyte, and a platinized counter electrode in a sandwich configuration. Improving the light-harvesting efficiency and suppressing the carrier recombination process at the semiconductor/electrolyte interface are two key factors to improve the performance of the UV-PDs. And various approaches to enhance light-harvesting efficiency have been reviewed in this sub-session, including porous films, length-wise NRAs, density-wise NWAs, 3D micro-/nano-architectures.

3.4.1.1 Porous films Once entering a porous NP layer, the incident light can be generally divided into two parts: (i) one part is adsorbed by NPs, (ii) the other part is penetrating the NP film after multiple refractions, which can increase the light harvesting. Then, based on this point, Mridha *et al.*[85] prepared a type of sponge-like porous ZnO with assistance of activated carbon (AC). This AC-assisted ZnO (AC-ZnO) shows SSA of 3.17 $m^2 g^{-1}$, which is increased 33% compared to that of the bare ZnO (B-ZnO). The UV absorption of AC-ZnO in the range of 300-400 nm is enhanced 10% compared to that of B-ZnO. Moreover, the S of AC-ZnO is 162, which is four times greater than that of B-ZnO. And both t_r and t_d of AC-ZnO are 5-6 times shorter than those of B-ZnO, indicating a fast photoresponse. Moreover, Hu *et al.*[86]

fabricated a type of mesoporous TiO_2 photoanodes via a gel hydrothermal method using PVP as pore-forming agent. It is found that the absorbance of TiO_2-1.5 wt% films is enhanced 23% in UV region compared to that of the dense TiO_2 films, implying the multiple refractions can greatly enhance the light absorption efficiency in TiO_2 photoanodes. And the counterpart PEC cells yields a η of 9.86%, which is enhanced 53.8% compared to that of the dense TiO_2 ones. This enhancement in η suggests that the porosity and pore size of TiO_2 photoanodes not only enhance light harvesting efficiency, but also affect the SSA of photoanodes for greatly enhanced electrolyte ion adsorption and interfacial charge transfer. Furthermore, Lei *et al*.[53] studied the effect of pore size on the optoelectronic performances of the porous films prepared via sol-gel technique using polystyrene (PS) spheres templates. Under UV illumination (369 nm, 32 mW cm^{-2}), the J_p of the arrayed 190-nm-pore films is 10 μA cm^{-2}, which is ~ 5 and 10 times as high as those of the 850-nm-pore and nonporous films. The sample with smaller pore size has larger SSA and is more effective for the improvement of the photocurrent.

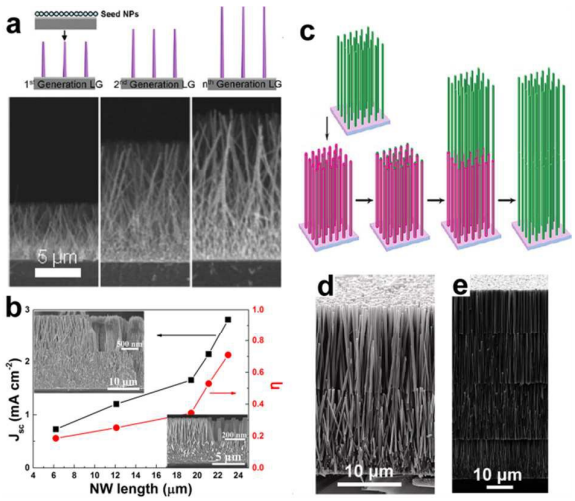

Fig. 7 (a) Schematic growth route for ZnO NWAs with different NW lengths, the bottom shows their SEM images. (b) J_{sc} and η of ZnO NWAs as a function of NW length, and the inset SEM images show the morphology change of ZnO NWs. (c) Schematic process for synthesizing multiple-layer assembly of ZnO NRAs, and (d-e) SEM images of two- and four-layer assembly of ZnO NRAs, respectively. (a) and (c-e) Reproduced from ref. 78 and 88, respectively. Copyright© 2011 American Chemical Society. (b) Reproduced from ref. 87. Copyright© 2014 Elsevier Ltd.

3.4.1.2 Length-wise NRAs Generally, the insufficient SSA of NWAs constrains the J_{sc} to

relatively low levels due to their low light absorbance. Ko *et al.*[78] performed a parametric study about the effect of NWA length on the efficiency of the photoanodes (Fig. 7a), and found that as the length of ZnO NWAs increases from 7 to 18 μm, the J_{sc} and η values are enhanced by 90% and 89%, respectively. This increase in J_{sc} and η is mainly due to effective SSA increase. Moreover, Xie's group also studied the effect of NWA length on J_{sc} and η (Fig. 7b),[87] and found that with increasing the length of the NWAs from 6 to 23 μm, the J_{sc} and η values are enhanced by 285% and 283% respectively. It is noted here that the η increases by 85% when the NWA length increases from 6 to 19.4 μm, while increases by 105% when the NWA length increases slightly from 19.4 to 23 μm. This increasing rate of enhancement is found to be due to the formed porous structure of ZnO NWs by etching during the long-time hydrothermal growth process. To avoid this situation, Xu *et al.*[88] demonstrate a convenient approach for synthesizing multilayer assemblies of ZnO NWAs (Fig. 7c-e), and found that the assembled four-layer ZnO NWAs possess an internal SSA more than 5 times larger than that of single-layer NRAs, and yield a high η of 7%, which is ~2.3 times higher than that of single-layer NRAs.

3.4.1.3 Density-wise NWAs Except length, the density of NW in an array can also affect the optoelectronic performance of the electrodes, especially, light absorption in visible region due to light scattering, which is unfavorable to UV detecting. Hu *et al.*[90] designed various density of ZnO NRAs using square patterns, and found that the patterned ZnO NRAs show a slight increase in UV absorption, while a large increase in visible absorption. Thus, suitable density of NWA is required for low absorption in visible region. In view of this point, Xie's group have prepared a type of dense dendriform TiO_2 (D-TiO_2) NWAs to serve as the photoanode of PEC self-powered UV-PDs.[45] The aspect ratio of the NWs is up to 150 and the surface density is about 90–110 NW μm^{-2}. The grown branches possess a cone shape with an average length of 80 nm and a base diameter of about 15 nm, densely filling the interspace

between TiO_2 NWs. The UV light absorption of D-TiO_2 NWA films is enhanced ~45% compared to that of TiO_2 NWA, and with a very low light absorption in visible region. And under UV light illumination (330 nm), the J_{sc} of D-TiO_2 NWA films is respectively enhanced 176% and 46% compared to those of TiO_2 NWA and nc-TiO_2 films. Especially, the responsivity in the visible region drops 1/396 for J_{sc} as compared with the peak value, indicating a visible-blind property. Under UV illumination (365 nm, 25 mW cm^{-2}), J_{sc} value exceeds 570 μA cm^{-2} with R_i of 22.8 mA W^{-1} and S of 1902. And, the t_r and t_d of the D-TiO_2 NWA based PEC cell are ~ 5.3 and 5.9 ms for J_{sc}, which is much faster than the photoconductivity-based UV detectors made by 1D TiO_2 nanostructures.[2, 74] In addition, the J_{sc} increases linearly with increasing the UV light intensity in a wide variation range from 0.05 to 27 mW cm^{-2}, showing a potential application for measuring UV intensity.

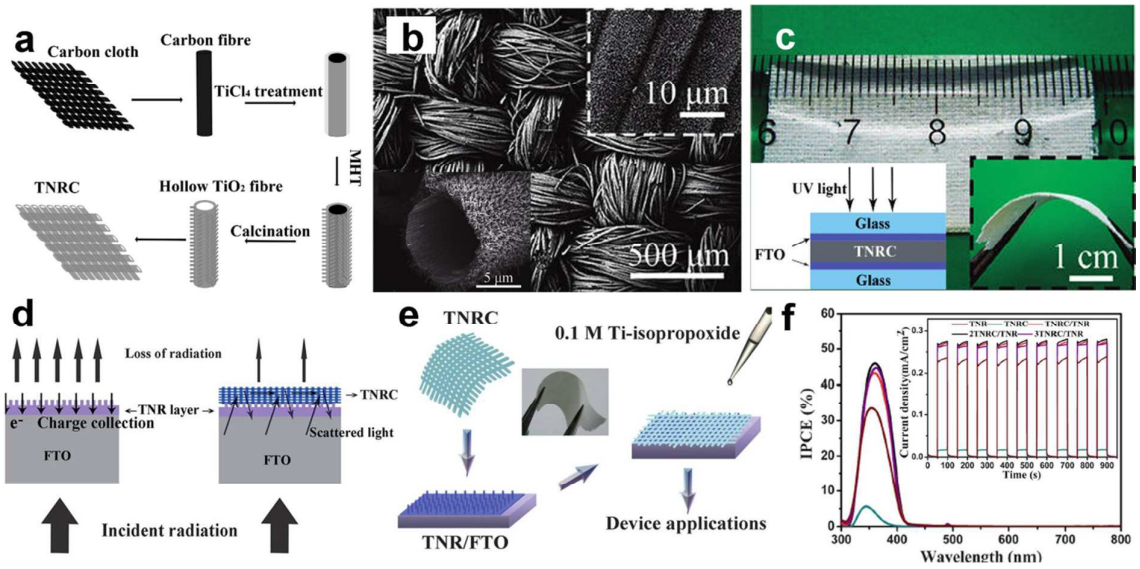

Fig. 8 (a) Scheme for fabricating the TNRCs, (b) top-view SEM image of the TNRCs, insets shows enlarged top and cross-sectional view SEM, respectively, and (c) optical images of TNRCs under a ruler, and the inset (right) shows their optical image under bending. (d) Design and principle for TNRC/TNR structure to achieve better performance, (e) scheme for fabricating TNRC/TNR structure, and (f) IPCE testing for the PEC PD, and inset show photoresponse of different PEC detectors under UV light rectangle pulse (365 nm, 1.55 mW cm^{-2}). (a-c) Reproduced from ref. 89. Copyright© 2011 American Chemical Society. (d-f) Reproduced from ref. 35. Copyright© The Royal Society of Chemistry 2012.

3.4.1.4 3D hierarchical architectures Recently, Shen's group have reported a type of flexible and transferable TiO_2 NRs cloths (TNRCs) synthesized using carbon cloths as

sacrificial templates, as illustrated in Fig. 8a.[89] The as-synthesized TNRCs are assembled by numerous aligned TiO_2 NRs with diameters of about 100 nm (Fig. 8b), showing good transferability and flexibility (Fig. 8c). Illuminated by UV light (365 nm, 1.25 mW cm^{-2}, -1 V), the assembled sandwich device without electrolyte show R of only ~ 10 mA W^{-1}, t_r of ~ 1.4 s, and t_d of ~ 6.1 s. These low optoelectronic performances are due to the relatively lower film thickness and NR density comparing to the traditional NP films, a large proportion of the photons will become transmission loss for TNRCs. Then, Shen's group further tried to combine multilayer of TNRCs with vertical TiO_2 NRs (TNRs), and obtained a type of 3D hierarchical TNRC structures.[35] It is found that the use of the hierarchical 3D TNRC structures can greatly reduce the "transmission loss" problem in TNRC films (Fig. 8d-e). And the IPCE of the TNRCs combined with TNRs increases from ~32.5% to ~ 45% at ~360 nm. Although the spectral response range is slightly widened, the photoresponse is still narrow enough to meet the ''visible blind'' property (Fig. 8f). Under UV illumination (365 nm, 1.55 mW cm^{-2}, inset of Fig. 8f), the PEC UV-PDs based on TNRC@TNRs using I^-/I_3^- electrolyte show a much higher photoresponse of 278 μA cm^{-2} with R of 179 mA W^{-1}, which is enhanced 18% compared to that of TNRs. Moreover, the t_r and t_d of TNRC@TNRs are 0.3 and 0.2 s, respectively. This indicates that introducing TNRC into UV-PDs increase the photoresponse by reducing light transmission, while retaining the carrier transport efficiency. Furthermore, all devices can not only response to very weak optical signals, but also show highly-linear properties, which can make them ideal candidates for UV radiation-level measurement. However, the 30% increase in light absorption only lead to a 12% increase in IPCE, which is mainly due to the poor attachment existing between the TNRCs and the TNRs. Nevertheless, this type of freestanding multilayer nanostructured photoanodes opens a new vista for fabricating high quality UV-PDs with fast and high response.

3.4.2 Enhancing charge separation or reducing charge recombination

Interfacial charge recombination is a problem that exists in PEC cells and causes a loss of photogenerated electrons.[75] Recently, semiconductor core-shell structures with type-II band alignment have attracted significant attention as the elementary building blocks for the fabrication of next generation electronics, because of their rapid carrier separation/injection to the photoanodes.[91] In core-shell structures, it requires that the CB's potential of the shell should be more negative than that of the core, which will establish an energy barrier at the semiconductor/electrolyte interface. Then, this established energy barrier can help the photogenerated carriers' separation and thus suppress interfacial charge recombination. According to the energy levels shown in Fig. 2, the core-shell structures of ZnO@TiO_2, ZnO@NiO, ZnO@ZnS, TiO_2@$SrTiO_3$ and SnO@TiO_2 possess great potentials in high-performance PEC devices.

3.4.2.1 ZnO-based core-shell structures The high I_d in ZnO nanostructured photoanodes caused by photo-corrosion in aqueous solution will greatly limit the photosensitivity of the devices. Thus, coating a layer of TiO_2 on ZnO nanostructures can effectively protect the ZnO NWs from degradation and corrosion in basic media under light illumination.[92] Moreover, it is also demonstrated that the I_d was largely blocked and the J_{sc} was increased because of the CB offset of 0.1 eV and VB offset of 0.2 eV between ZnO core and TiO_2 shell (Fig. 9b).[93-95] In 2013, Xie's group reported a type of PEC UV-PDs based on ZnO@TiO_2 core-shell nanostrawberries (ZnO NS-TiO_2) using the traditional I^-/ I_3^- electrolyte (Fig. 9a).[29] The resultant TiO_2 shell is 3 nm in thickness (inset of Fig. 9d), and the ZnO-NS core are ~250 nm in length, ~155 nm at big side, ~91 nm at small side, consisting of ~22-nm rod-like NPs (SEM image in Fig. 9c). Under the UV illumination (365 nm, 20 mW cm^{-2}, Fig. 9d), the ZnO NS-TiO_2 based device gives a high J_{sc} of 357 μA cm^{-2} with R_λ of 17.85 mA W^{-1}, which is enhanced 52.5% compared to that for the ZnO-NS based one, indicating an improved R_λ. And, the S of the J_{sc} signal from ZnO NS-TiO_2 based devices is ~ 37,900, which is 3.24 times as

high as that from ZnO-NS based ones. The t_r and t_d are estimated to be 0.022 and 0.009 s for J_{sc}, respectively. Moreover, J_{sc} increases linearly with increasing the 365-nm UV light intensity in a wide variation range from 0.002 to 40 mW cm^{-2}.

Except TiO_2, other wide-band-gap semiconductors, such as NiO and ZnS, can also be applied to enhance the optoelectronic performances of ZnO-based nanostructures. NiO (p-type, 3.7 eV) can easily form p-n heterojunction with n-type ZnO and generate an inner electric field at their interface of heterostructures. Dai *et al.*[63] constructed a type of honeycomb-like ZnO@NiO core-shell NRAs via a photochemical deposition process, and found that the *S* of ZnO@NiO-NRA based PDs is as high as 167, which is nearly enhanced by 49 folds compared with the bare ZnO NRA under 365-nm UV illumination. And, both t_r and t_d from ZnO@NiO NRAs are also greatly decreased to 1/7 of those from the ZnO NRAs. As for ZnS, it is also a wide-band-gap material with especially high CB position, which can produce excitons with strong driving force for reactions. Guo *et al.*[42] found that ZnO@ZnS NRAs show similar UV light absorption with ZnO NRAs, but with higher transmittance in visible light region, which is favorable to UV detecting. And under UV illumination (0 V bias), the J_{sc} of ZnO@ZnS NRAs is enhanced over 100% compared to that of ZnO NRAs, which is mainly due to the high separation efficiency of photogenerated carriers.

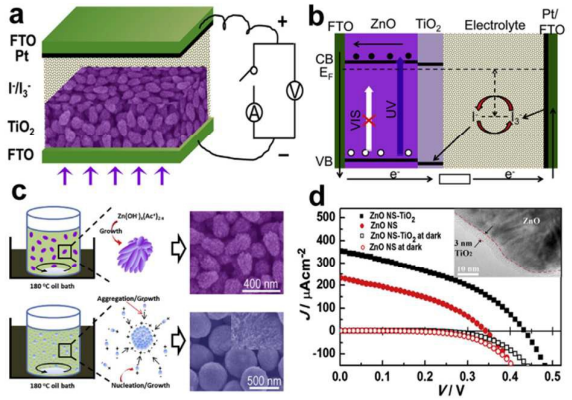

Fig. 9 (a) Schematic of self-powered UV-PDs based on ZnO NS-TiO_2 films, (b) energetics of operation of the UV-PDs, (c) Schematic diagram of the formation mechanism of strawberry-like and sphere-like ZnO aggregates, the right insets are their corresponding SEM images, and (d) *J-V* curves of the self-powered UV-PDs based on ZnO NS-TiO_2 and ZnO NS films. Inset is HRTEM image of ZnO NS-TiO_2 taken from ZnO/TiO_2 interface. Reproduced from ref. 29. Copyright© 2013 Elsevier Ltd.

3.4.2.2 TiO_2-$SrTiO_3$ core-shell structures TiO_2 is one of the most commonly used materials in the photoanodes for PEC cells, but it shows low electron mobility, leading to slow electron diffusion transport and high recombination. It is expected that the heterojunction of photoanodes could facilitate the separation or suppress the recombination of photogenerated carriers at the semiconductor interface, resulting in the final high efficiency of the photoanodes. $SrTiO_3$ is one wide-band-gap (3.4 eV) optoelectronic ceramic material, which possess a high PEC activity. Kim *et al*.[46] fabricated a type of TiO_2@$SrTiO_3$ core-shell heterojunction NTAs by anodization of Ti foils and sequential hydrothermal reaction. The maximum η of the TiO_2@$SrTiO_3$-1 h NTAs is 6.6%, which is enhanced 65% compared to that of the bare TiO_2 ones. Under UV illumination (250-385 nm), they exhibit a quick and repeatable photoresponse with J_P of ~650 μA cm^{-2}, which is 3-fold that of the bare TNTAs. This enhancement is mainly because of their charge separation and suppression of charge recombination at the $SrTiO_3$/TiO_2 interface.

3.4.2.3 SnO_2-TiO_2 core-shell structures Thus far, it is demonstrated that the application of SnO_2 to PEC cells has been greatly limited due to its poor PEC behaviors, which primarily arises from a larger interfacial electron recombination and lower trapping density. To settle down this problem, many researchers have tried to coating of TiO_2 nanostructures onto SnO_2 cores. This combination can simultaneously solve the large interfacial electron recombination of photogenerated carriers in SnO_2 and the slow diffusion transport of electrons in TiO_2 (Fig. 10c and h), which are mainly due to two aspects: 1) SnO_2 possesses higher electron mobility (~ 100 to 200 cm^2 V^{-1} s^{-1}) than TiO_2 (~ 0.1 to 1.0 cm^2 V^{-1} s^{-1}), which can work as oriented charge transport path,[64] and 2) TiO_2@SnO_2 core-shell structure can yield a surface dipole layer toward SnO_2, which can benefit to suppressing interfacial charge recombination.[81, 96-98] Xie's group reported a type of branched nanostructures of TiO_2 nanoneedles on SnO_2 NF network (B-SnO_2), and applied this type of B-SnO_2 in the photoanodes for PEC UV-PDs (Fig.

10a-b).[28] Under UV irradiation (330 nm), the η of PDs reaches 14.7%, which is over twice as big as that of nc-TiO_2 films (6.4%), indicating that these branched heterojunction nanostructures can simultaneously exhibit a low degree of charge recombination and work as a direct pathway for electron transport. And under UV illumination (365 nm, 40 mA cm^{-2}), the PDs exhibit a J_{sc} of 900 μA cm^{-2} with R_λ of 22.5 mA W^{-1}, S of ~4550, t_r of 0.03 s, and t_d of 0.01 s for J_{sc} signals. Moreover, a type of branched TiO_2 nanoneedles on SnO_2 NS (SnO_2 NS-TiO_2) was further applied in PEC UV-PDs (Fig. 10d).[47] These SnO_2 NS-TiO_2 electrodes are highly transparent and show a "visible-blind" characteristic (Fig. 10e). Under UV irradiation (365 nm, 40 mW cm^{-2}), the UV-PD shows a J_{sc} of 709.5 μA cm^{-2} with R_λ of 17.73 mA cm^{-2}, S of 440.5 for J_{sc} signal, and fast photoresponse (0.02 s for t_r and 0.004 s for t_d). These results indicate that this ultrathin SnO_2 NS core can serve as the fast electron transport network for fast photoresponse, but at the same time also cause high electron recombination at their grain boundaries that leads to a low R_λ. Then, Xie's group further assembled SnO_2 NSs into a type of SnO_2@TiO_2 core-shell hierarchical hollow nanospheres (HNSs) (Fig. 10f),[31] in which the TiO_2 shell consists of large number of tapered TNRs with length of over 10 nm (Fig. 10g). The assembled UV-PDs show the maximum value of R_λ at 330 nm, which is 12.4 times as high as that of SnO_2 HNS films, 1.1 times as high as that nc-TiO_2 films, even 39.5% higher than the above B-SnO_2 NFs.[28] Under UV illumination (365 nm, 35 mW cm^{-2}), the J_{sc} from SnO_2@TiO_2 HNS based PDs exceeds 1277 μA cm^{-2} with R_λ of 35.05 mA W^{-1}, S of ~ 4020, t_r of 0.03 s, and t_d of 0.01 s. This great enhancement is mainly due to multiple reflecting and scattering of light in the hollow spheres and the decrease of electron recombination at grain boundaries, which may lead to high light trapping and carrier generation efficiencies.[99, 100] Besides, Shen's group has prepared a type of freestanding SnO_2@TiO_2 core-shell heterostructure microtubes using carbon cloth as templates (Fig. 10 i-j).[32] The TiO_2 shell consists of rutile TiO_2 NRs and shows a superior synergistic effect on

electrochemical performances. Under UV illumination (365 nm, 1.55 mW cm^{-2}), the assembled PEC UV-PDs show a high J_p of 100 μA cm^{-2} with R_λ of 64.5 mA W^{-1}, which is enhanced 22% compared to that of the pure SnO_2 one. This enhanced photoresponse performance is due to effective charge separation and good transport that achieved in the SnO_2@TiO_2 cloth.

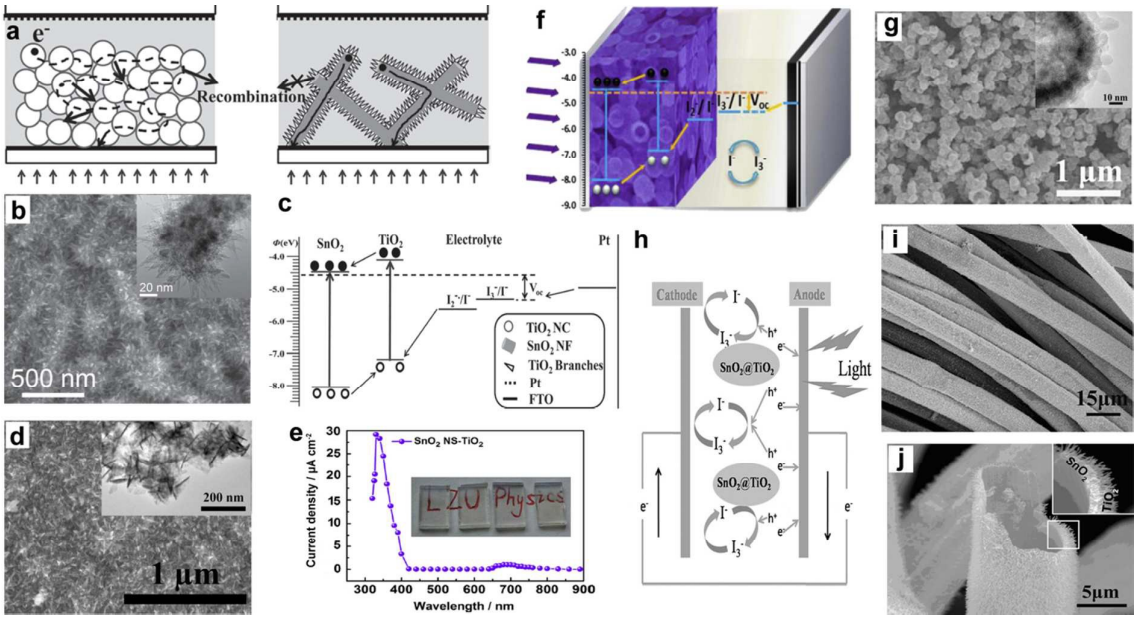

Fig. 10 (a) Diagram for self-powered UV-PD based on nc-TiO_2 (left) and B-SnO_2 NF films (right), (b) SEM image of B-SnO_2-NF films, and inset is its TEM image, (c) energetics of operation of B-SnO_2-NF UV-PD. (d) Top view image of SnO_2 NS-TiO_2 films, and inset is its TEM image, and (e) spectral response of the self-powered UVPDs, inset is the digital photograph of transparent SnO_2 NS-TiO_2 films. (f) Structure scheme of UV-PDs based on SnO_2@TiO_2 HNSs, (g) SEM images of SnO_2@TiO_2 hierarchical HNSs, the insets show the TEM image. (h) Detailed carrier transferring process of the PEC cell under illumination, (i) SEM images of SnO_2 NP-TiO_2 NRs composites, (j) cross-sectional view SEM of SnO_2@TiO_2 microtube. (a-c) and (h-j) Reproduced from ref. 28 and 32, respectively. Copyright© 2012 and 2014 Wiley-VCH. (d-e) and (f-g) Reproduced from ref. 47 and 31, respectively. Copyright© 2014 Elsevier Ltd.

3.4.3 Enhancing charge transport efficiency in photoanodes

It has been recognized that diffusion is the major mechanism for electron transport in the oxide films, while multiple trapping/de-trapping at the grain boundaries usually result in a decreased electron transport rate in the oxide films.[62, 84] Since the electrons in the photoanode would be easily recombined with oxidized ions (such as I_3^-) in the electrolyte, the transit time of electrons within the oxide films should be much shorter than the time needing for their

recombination, i.e., life time. Thus, to enhance charge transport efficiency is another key factor for increasing the PEC performances of a PD.

3.4.3.1 NP/1D nanostructure hybrids Compared to NPs, 1D NWs or NRs usually possess the advantages of fast electron transport rate and excellent light scattering. However, at the same time, these two nanostructures suffer from their low SSA which usually results in a low light absorption efficiency and hence leads to low J_{sc} and R_{λ}.[101, 102] Zhang *et al*.[52] assembled anodic TiO_2 NTA/NP composites into photoanodes. Compared to the bare TNTAs, the TNTA/NP composites exhibit a visible-blind characteristic but with a slight red shift in absorption edge. Moreover, this type of NTA/NP photoanodes show a fast photoresponse to UV light (200-400 nm), and the J_{sc} is increased 29% compared to that of the bare TNTAs. These improvements in their PEC performances could be mainly due to the higher separation efficiency of the photogenerated electron-hole pairs and effective charge transport between the TiO_2 NTs and NPs.

3.4.3.2 Reduced NRAs Surficial reduction can greatly increase the donor density of oxide nanostructures, which can benefit the photogenerated carrier transport. Yao *et al*.[103] prepared a type of hydrogenated ZnO hierarchical NRAs (H-ZnO HNRAs) by a two-step electrochemical process. After hydrogenation annealing, the color of the white ZnO HNRA film changes to black H-ZnO HNRAs. The carrier density of H-ZnO HNRAs is enhanced over 14 folds compared to that of the pristine ones, and H-ZnO HNRAs show a broad UV photoresponse from 300 to 370 nm with IPCE of more than 90%. Similar results can also be reviewed from the work by Xu *et al*.[60].

Moreover, it is raised that the existence of Ti^{3+} defects (oxygen vacancies) in bulky TiO_2 nanostructures can enhance their electrical conductivity.[104] In this case, Ti^{3+}-induced mid-gap states, as shallow donor sites, could contribute to the charge density enhancement and narrowed band gap, and lead to further improved PEC efficiency.[105] Zhang *et al*.[106] reported

the preparation of reduced TNTs (r-TNTs) using the electrochemical doping via cathodic reduction. The r-TNTs show a visual change of color from grey to dark blue, and their charge transfer resistance decreases from 1246 to 90.79 Ω cm^{-2}. And the J_p of r-TNTs increases by 33.3% compared to that of the pristine TNTs under UV irradiation (375 nm, 300 mW cm^{-2}).

3.4.3.3 Element doping Doping suitable elements into TiO_2 is found to be important for the reduction of the photogenerated hole-electron recombination rate.[107] Wang *et al*. fabricated nitrogen-doped TiO_2 mesosponge (N-TMSE and N-TMSW) by transformation of TNTAs using a solvothermal method (Fig. 11a).[57] The color of TNTAs changes from the original grey to sky-blue after doped with N elements, which corresponds to higher light absorption in UVA region. Under UV irradiation (254 nm, 500 W) in 0.1 M Na_2SO_4 electrolyte, the saturated J_ps of N-TMSE and N-TMSW are respectively ~427 and 370 μA cm^{-2}, which are much higher than that of the pristine TNTAs (318 μA cm^{-2}). The improved J_p could be mainly because N doping facilitates the separation and transfer of photogenerated electron/hole pairs. Moreover, Xu *et al*.[60] doped Sn elements into TiO_2 NWs by a one-pot hydrothermal synthesis. The obtained Sn-doped TiO_2 (Sn/TiO_2) NWs with Sn/Ti ratio of 1−2% are single crystalline with a rutile structure. The Sn/TiO_2-12 NW photoanodes shows a high J_p of 2.0 mA cm^{-2}, which is enhanced 100% compared to the best pristine TiO_2 NW photoanodes. This increase in photocurrent density is mainly ascribed to the enhancement of photoactivity in the UV region and the significantly improved density of n-type carriers by Sn doping.

Although suitable mono-doping (single element doping) can enhance the PEC performance of TiO_2 to some extent, while excessive mono-doping will increase carrier recombination centers and reversely decreases the overall PEC performance. Then, a new type of donor-acceptor co-doping concept was proposed to improve the PEC performances of TiO_2 photoanodes.[109] This type of co-doping TiO_2 with donor-acceptor pairs can not only

enhance the charge transport, but also reduce charged defects and their associated recombination, and accordingly improve their PEC performances. Dong's group reported a type of bimetallic Au-Pt NP/NH_2-group functionalized TiO_2 hybrid nanoparticles (noted as f-TiO_2-Au/Pt NPs) via a simple self-assembly approach.[110] These f-TiO_2-Au/Pt NPs consist of evenly dispersed Au/Pt NPs (6-7 nm) on f-TiO_2 colloid spheres with nanoporous surface. Under UV illumination (365 nm), the f-TiO_2-Au/Pt NPs show a stable I_p of 0.30±0.02 μA, which is about 4-fold that of the f-TiO_2 NPs (0.08±0.03 μA). Moreover, Cho *et al*. reported a novel ex-situ method to co-doped TiO_2 with W and C elements by sequentially annealing W-precursor-coated TiO_2 NWs in carbon monoxide gas (Fig. 11b).[108] The integrated UV light absorption (plus scattering) values of (W, C) co-doped TiO_2 NWs is enhanced only 7.56% compared to that of the undoped ones, while the IPCE value of the co-doped TiO_2:(W, C) NWs is ~80% at 380 nm, which is enhanced 150% compared to that of the higher undoped TiO_2 (~32% at 395 nm). And the saturation J_p of the co-doped TiO_2:(W, C) NWs is 2.4 times as high as that of the undoped TiO_2 NWs. These enhancements suggest that the co-doping with donor-acceptor pairs can greatly enhance charge separation and transport efficiency. Interestingly, the co-doped TiO_2:(W, C) NWs also shows very fast photoresponse to UV light.

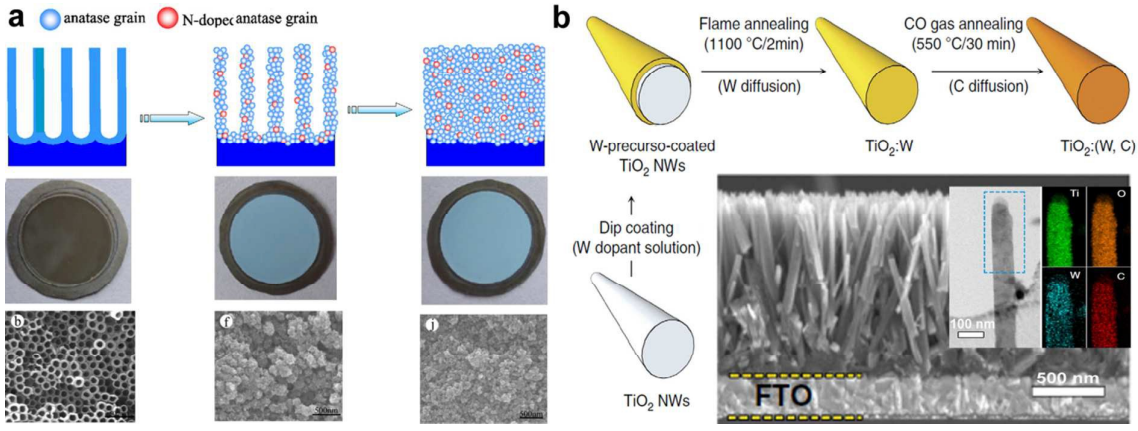

Fig. 11 (a) Transformation processes of NTs into mesosponge of TiO_2 by solvothermal treatment in ethanol solution of ammonia, and their corresponding optical and SEM images (top views). (b) Schematic illustration of the preparation of TiO_2:(W, C) NWs by ex-situ doping method; the bottom is cross-sectional SEM image, the inset shows TEM and EDX mapping images. (a) Reproduced from ref. 57. Copyright© 2012 Elsevier Ltd. (b) Reproduced from ref. Cho, et al. 108. Copyright© 2013 Nature Publishing Group.

3.4.3.4 Optics–electrics highways Recently, conductive nanostructures modified technology has been employed as a promising way to boost the performances of PEC cells via optics–electrics highways.[111-114] It has been applied to significantly accelerate the carriers' transport and separation, and hence considered to be one of the most attractive technologies to improve the η. Dong *et al.*[112] first proposed a concept of "optics–electrics highways" using a type of bristled silver NWs@TiO_2 core–shell nanostructures (Fig. 12a). It is demonstrated that these constructed composites significantly accelerate electron transport as well as reduce recombination, then greatly improve the charge collection efficiency of the cells, and accordingly enhance the IPCE by 43%. However, this type of metal nanostructures can often generate localized surface plasmon resonance, which can not only enhance light harvesting in UV region, but also greatly increase the photoresponse in visible light region.

Carbon nanostructures, such as single-walled carbon nanotube (SWCNT), were also used as conducting scaffolds in a TiO_2-based PEC cells, in which TiO_2 nanoparticles were dispersed on SWCNTs (Fig. 12b-c).[58] Compared to the undoped TiO_2 cells, the SWCNT/TiO_2-based cells show a great increase (over 200%) in J_p and/or η values, indicating the beneficial role of the SWCNT as conducting scaffold to facilitate charge transport in TiO_2 films. Meanwhile, multi-walled carbon nanotubes (MWCNTs) were also incorporated into rutile TiO_2 NWAs.[55] It is found that with increasing MWCNT content, the absorption edges of the TiO_2@MWCNT NWA films are slightly blue-shifted with wavelength of ~ 10 nm. And the maximum η was observed from the 0.1-MWCNT-TiO_2 NWA films, and it is enhanced 194% compared to that of the undoped ones. Further EIS results suggest that the small amount of MWCNT would promote the photogenerated electron transfer, thus enhance the PEC performances of the devices. However, like mono-element doping, excessive MWCNT contents can also increase the trap state formation, and thus photogenerated electrons would spend more time to reach the FTO substrate.

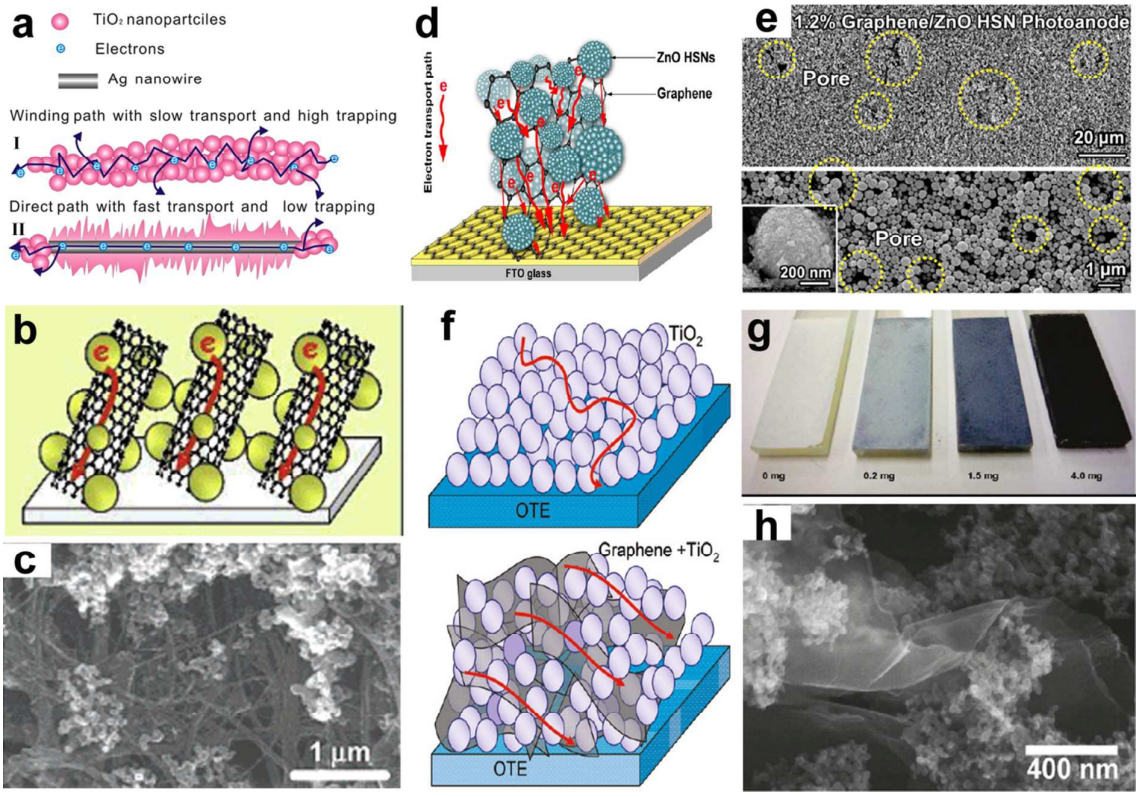

Fig. 12 (a) Schematic diagram of photoelectrons transport in photoanodes of (I) pure and (II) Ag NW-modified TiO_2. (b) Schematic illustrations of electron transport across SWCNT-doped TiO_2 films, and (c) SEM images of SWCNT/TiO_2 films. (d) Schematic diagram of graphene/ZnO HSN composite photoanode and possible electron transport path within the structure; and (e) top-view SEM images of graphene/ZnO HSN composites (~1.2 wt % graphene loading), the inset is the magnified image of an individual ZnO HSN. (f) Schematic illustrations of electron transport in pristine TiO_2 (upper) and r-GO-TiO_2 (lower) nanocomposites, (g) photographs of TiO_2 films with different r-GO loadings, and (h) SEM image of r-GO-TiO_2 nanocomposites. (a) Reproduced from ref. 112. Copyright© 2014, Elsevier. (b-c), (d-e) and (g-h) Reproduced from ref. 58, 115 and 51, respectively. Copyright© 2007, 2013 and 2010 American Chemical Society.

Graphene is another type of carbon nanostructures that can also be used to enhance electron transport properties of oxide photoanodes. Compared to CNTs, reduced graphene oxide (r-GO) can provide a 2-D conductive support path for charge transport and collection at the electrode surface (Fig. 12f). In view of this point, Kamat's group synthesized a type of r-GO-TiO_2 nanocomposites via a solution-based method involving photocatalytic reduction of GO.[51] The color of TiO_2 thin films gradually changes from white to black with increasing the addition of r-GO (Fig. 12g-h). The r-GO-TiO_2 composites exhibit the maximum η value of 13.9% at ~350 nm, which is enhanced 87.8% compared to that of the pure TiO_2 films (7.4%). Upon UV irradiation (320-400 nm, 100 mW cm^{-2}) in 1 M KOH electrolyte, the

r-GO-TiO_2 films (with r-GO of 0.05 mg cm^{-2}) output a J_p of ~38 μA cm^{-2}, which is enhanced 90% compared to that of the TiO_2 films (~20 μA cm^{-2}). These observed enhancements in the photocurrent and IPCE represent improved charge transport from r-GO-TiO_2 nanocomposites to the collecting electrode surface. Similar results can also be reviewed from the work by Xu et al.[115], in which graphene was incorporated into ZnO nanoparticle photoanodes (Fig. 12d). After incorporated 1.2 wt% graphene into the 3-μm-thick ZnO hierarchical structured nanoparticle (HSN) photoanode (Fig. 12e), the assembled devices exhibit a high J_{sc} of 10.89 mA cm^{-2} and η of 3.19%, which are increased by 43.48% and 38.09%, respectively, compared to those of the devices without graphene. Moreover, it was also found that the incorporation of graphene into electrodes could not only effectively decrease the internal resistance within the photoanodes, but also markedly prolong electron lifetime and effective diffusion length. This allows the utilization of thicker photoanodes that could afford enhanced SSA for light harvesting, and an impressively high η of 5.86% was achieved for the 9-μm-thick ZnO HSN photoanode. However, like the case of MWCNTs, excessive r-GO loadings will adversely affects the electron transport in the composite films. And the incorporated graphene can cause more oxygen-related defects in the ZnO HSN photoanode, which often show an enhanced visible light absorption.

3.5 Recent multi-functional PEC UV-PDs

3.5.1 Wearable ZnO NRA/metal wire microcells Recently, Yu's group reported a prototype of double-sided, transparent, flexible, ITO-free PEC cells,[116] in which hierarchical ZnO NWAs (200 nm in diameter, 2 μm in length, and 5000 mm^{-2} in density)/metal microwire (stainless steel, Au, Ag, and Cu) serves as working electrodes, and Pt wire serves as the counter electrodes (Fig. 13a). This device shows good transparency and can increase light harvesting efficiency via two-side illumination (Fig. 13b). Moreover, the double-wire cells

remain stable for a long period of time and can be reversibly bent under large angles, even to 107°, but without any loss of performance. However, the untreated metal wires can usually be electrochemically corroded by the electrolyte ions, leading to a high J_d of 2.03 mA cm^{-2}. Thus, an oxidation treatment to the metal wires is developed effectively to avoid the electrochemical corrosion in the experiment and to fasten the light response, which is crucial for real applications of double-metal-wire PEC devices. This double-wire-PET, planar solar-cell configuration can be used as various flexible PEC devices, such as PEC UV-PD, and can be readily realized for large-area-weave roll-to-roll processes.

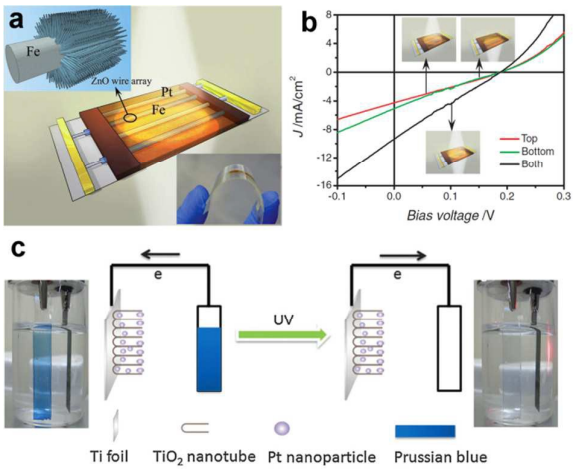

Fig. 13 (a) Schematic prototype of double-sided transparent PEC devices. The left inset shows hierarchical ZnO-NWA/Fe microwires, and the right one shows high flexibility of the device. (b) J-V curves of double-sided transparent cells under illumination from the top, bottom, and both sides. (c) General working principle of a self-powered, visual and self-recovered PD, the inset photographs show the color change of the PB/ITO ON/OFF UV illumination. (a-b) Reproduced from ref. 116. Copyright© 2012 Wiley-VCH. (c) Reproduced from ref. 117. Copyright© The Royal Society of Chemistry 2014.

3.5.2 Visual UV-PDs More recently, Dong's group reported a type of self-powered visual UV-PD with Prussian blue electrochromic display, in which Pt-modified TNTs and Prussian blue (PB)-modified ITO (PB/ITO).[117] Fig. 13c shows the general working principle of this visual UV-PD. Upon UV illumination, a number of electron–hole pairs are generated in TNTs. And the holes will oxidize water to oxygen, while the electrons will flow through an external circuit to the cathode, where PB will be reduced to Prussian white (PW) with color changing from blue to transparent. Thus we can judge the existence of UV light through the color

change of PB. And, Pt/TNT could also be used as the cathode in the dark. When connected with PW-modified ITO, the PW can be oxidized to PB whereas the electrons flow to the Pt/TNT cathode, which catalyzes oxygen reduction. Based on the discussions above, a self-powered, visual and self-recovered PD is achieved. These self-powered, visual and self-recovered UV-PDs make it possible to judge the existence of UV light easily by naked eye. More interestingly, it is also possible to fabricate a type of UV test cells based on this principle, similar to PH test paper.

3.5.3 Multi-functional UV-PDs with bi-polar electrodes Intelligent devices are attracting more and more attention during recent years. Generally, these so-called "intelligent devices" are the equipments that integrated with multiple functional components. On the other hand, introducing Bi-polar electrode (BPE) into those multiple functional optoelectronic platforms will make them become light-weight, low-cost, small size and portable. A BPE in optoelectronic devices can act as both the anode and cathode when two different cells are integrated in series. Chen et al. [118] reported a type of optoelectronic three-electrode system, in which a SC and a PEC cell were integrated and separated by sharing a common Pt electrode (Fig. 14a). This is the so-called "photocapacitor".[119] The photovoltage can rapidly increase and reach 90% of the maximum value (0.69 V) by illumination for 28 s. Moreover, Peng's group replaces Pt electrode with aligned CNT materials (Fig. 14b),[120] and found that the photovoltage can reach 90% of the maximum value (0.72 V) by illumination for less than 5 s, indicating a more efficient electron transport. Furthermore, Peng's group integrated CNT fibers and a Ti wire modified with aligned TiO_2 nanotubes on the surface into a optoelectronic device.[121] As shown in Fig. 14c, the Ti wire is used as BPEs for two cells and aligned CNT fibers were finally twisted with the modified Ti wire to produce the desired device. Upon the exposure to the light, the voltage can be charged to 0.6 V in few seconds, and the overall photoelectric conversion/storage efficiency is 1.5%. It is noted that this novel

wire structure can also enable unique and promising applications in wearable and portable PEC UV-PDs.

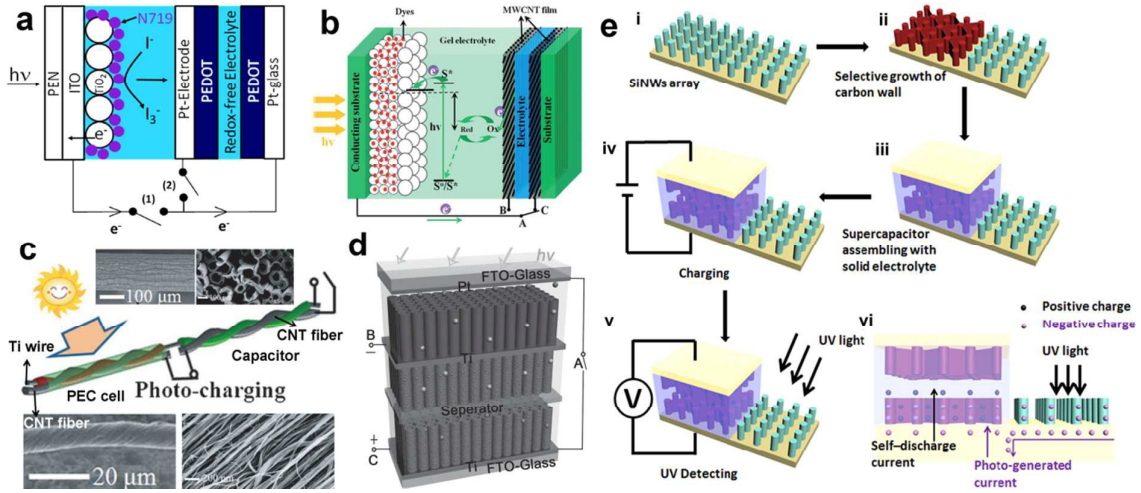

Fig. 14 (a) Configuration of optoelectronic device contains a DSSC and a polymer-based SC using Pt as BPEs. (b) Schematic illustration of a PEC cell/SC optoelectronic device using aligned MWCNT films as BPEs. (c) Schematic illustration of the wire-shaped device integrated a PEC cell/SC optoelectronic device using a Ti wire as BPEs. The upper insets show SEM images of a Ti wire coated with aligned TNTAs, the lower insets show SEM images of a CNT fiber. (d) Structure schematic illustration and work mechanism of a PEC cell/SC optoelectronic device using TNTAs as BPEs. (e) Fabrication process and structure of the bi-functional UV-PD. (a) Reproduced from ref. 118. Copyright© 2012 Elsevier Ltd. (b) Reproduced from ref. 120. Copyright© The Royal Society of Chemistry 2013. (c-d) Reproduced from ref. 121 and 122, respectively. Copyright© 2012 and 2014 Wiley-VCH. (e) Reproduced from ref. 123. Copyright© 2015 Elsevier Ltd.

More recently, Shen's group employed a BPE of TNAs into an optoelectronic integration.[122] As shown in Fig. 14d, 1D anodic titanium oxide (ATO) NTAs were used as the photoanode materials for PEC cells and hydrogenated ATO (ATO-H) NTA as the cathode materials for electrochemical SCs. On visible light illumination, a pulsed anodic photocurrent ~ 2.6 mA cm^{-2} occurred promptly and then gradually decayed to 0.025 mA cm^{-2} in 1 s. Consequently, a maximum, stable and repeatable charge voltage of 0.61 V is achieved on SC after being photo-charged for 1 s. These results indicate that this type of optoelectronic device can also show a rapid response to light, even to UV light. In view of this, Zhang's group tried to integrate a UV-PD with a supercapacitor (SC) on one vertical-aligned silicon NW (SiNW) array electrode,[123] in which carbon coated SiNWs were used as the electrode for the SC and the pristine SiNWs were used as the electrode for UV-PDs (Fig. 14e). The

assembled SC shows a capacitance density of 13.6 F cm^{-3}, which can be fully charged in 80–100 s and then support the UV-PDs for 10 h. Upon UV illumination (365 nm), the photoresponse can be observed from the external circuit potential increase (0.03–0.12 V) between the two electrodes of the SC. Although the reported UV detecting performances are not comparable to those from the above PEC UV-PDs, this type of self-powered multi-functional system that integrates power conversion/storage with UV light detecting will open a new insight for the design of multi-functional PEC UV-PDs.

4 Summary and outlook

In this review, we have discussed the recent progresses in self-powered PEC UV-PDs. Various nanostructures, including nc-films, NWs/NRs, NTs, NSs, NRAs, NTAs, nano-forest, etc., have been synthesized for photoanodes of PEC UV-PDs benefiting from their high UV light absorption, fast carrier separation/transport efficiencies, high spectral responsivity, high photosensitivity, and fast photoresponse. On the other hand, regarding electrolyte, I^-/I_3^-, water, Na_2SO_4 aqueous solution, etc., have been adopted, and the recent reported multi-functional PEC optoelectronic devices have been simply presented. However, current research work is still at the initial stage focusing on the designs for photoanode structures. And these reviewed researches are continuously developed according to the traditional optoelectronic devices (such as DSSC), involving device structure (sandwich structure), light harvesting, separation and transport mechanism of carriers, electrolyte, and counter electrode. In nature, the mechanism for PEC UV-PDs is highly different to those for other optoelectronic devices. However, several issues, such as light absorption mechanism under UV illumination, interfacial charge dynamics, and recombination mechanism of carriers, have not been investigated in detail. Thus, future endeavors are needed to achieve further improvement in the material and device designs, and photo detecting performances for practical applications.

The related outlook points are listed as below:

Photoanode structures Photoanode materials and structures are one of the most important components for the whole PDs, and greatly determine the light harvesting of a PEC cell. We can optimize the structures of photoanodes for PEC UV-PDs from the following aspects:

i) UV light absorption. Usually, one optoelectronic device requires a photoanode film with sufficient thickness to absorb light, which is dependent on the penetration depth of UV light. Excessive thickness of the film will result in the increase of diffusion length of photogenerated electrons. Thus, the optimized thickness of photoanode films is an important issue. On the other hand, light scattering can increase the light propagation length, which is one effective approach to improve the light harvesting efficiency. It is noted here that light scattering can also enhance the visible light absorption, which is unfavorable to the UV selectivity of a PD. Thus, we should modify the size of nanostructures according to the wavelength of the target UV light, in order to achieve an ideal scattering effect.

ii) Separation of photogenerated carriers. Under excitation by UV light, the electrons in the semiconductor will transit from the VB to CB, leaving a hole in the VB, which is subsequently reduced by ions in the electrolyte. Thus, first, it is necessary to guarantee adequate semiconductor/electrolyte interface area, i.e., for the efficient separation of carriers, thus requiring a large SSA for the nanostructures in photoanodes. Second, except for a high SSA, photoanodes should possess suitable pore size and porosity, which will benefit the diffusion of electrolyte to the whole films. It is also worth noting here that the penetration depth of UV light in semiconductor is about 2 μm, which is much less than that of visible light. Then the film thickness required by PEC UV-PD (1-2 μm) is far less than that of a DSSC (10 μm for P25). This is to say, compared to a DSSC, the PEC UV-PDs need smaller pore size in photoanode film to meet effective diffusion of electrolyte. Third, different crystal planes of semiconductors and size distribution of nanostructures will also affect this PEC

interfacial charge dynamics.[70]

iii) Transport of electron. Photogenerated carriers will be separated at the semiconductor/electrolyte interface, and the electrons that inject into the CB of semiconductor will diffuse through the photoanode to the collector. Then, the transport rate is the key factor to determine the efficiency of the electron collection and the response speed of a PD. It is demonstrated that 1D nanostructures with high crystallinity and high aspect ratio can provide direct transmission channel for electron, which can greatly reduce the electron recombination at the grain boundary during the transport.[78, 87, 88] And it is reported that the PEC UV-PDs assembled using TiO_2 NWAs with aspect ratio of 150 show greatly improved performances in photo detecting. However, up till now, few reports can be reviewed about the PEC UV-PDs based on high-electron-mobility and high-aspect-ratio semiconductors nanostructure such as TiO_2 or SnO_2. Besides, it is widely reported that conductive nanomaterials, such as CNTs, graphene, or metal nanostructures, can work as optics–electrics highways to boost the performance of PEC cells. Then, we believe that these strategies can also be used to enhance the performances of PEC UV-PDs.

iv) Reducing the recombination of photogenerated electrons. In a PEC UV-PD, the surface of semiconductor nanomaterial can directly contact with the electrolyte, which usually make the electrons that transit to the CB easily recombine with the electrolyte ions. The optics–electrics highways stated above can not only facilitate the transport of electrons, but also reduce the recombination of electrons. On the other hand, one more effective way is to make the semiconductor heterojunction (such as p-n junctions and Schottky junctions) and to form a type-II band structure, which can block electron recombination by the barrier. According to Fig. 2, many semiconductor heterojunctions, such as ZnO/ZnS, ZnO/NiO, $SrTiO_3/TiO_2$, etc., possess a high potential in PEC UV-PDs.

In brief, for an ideal photoanode, it is important to balance these four aspects above into

an integrated system, not just to prepare high-SSA nanostructures with amazing morphologies and structures.

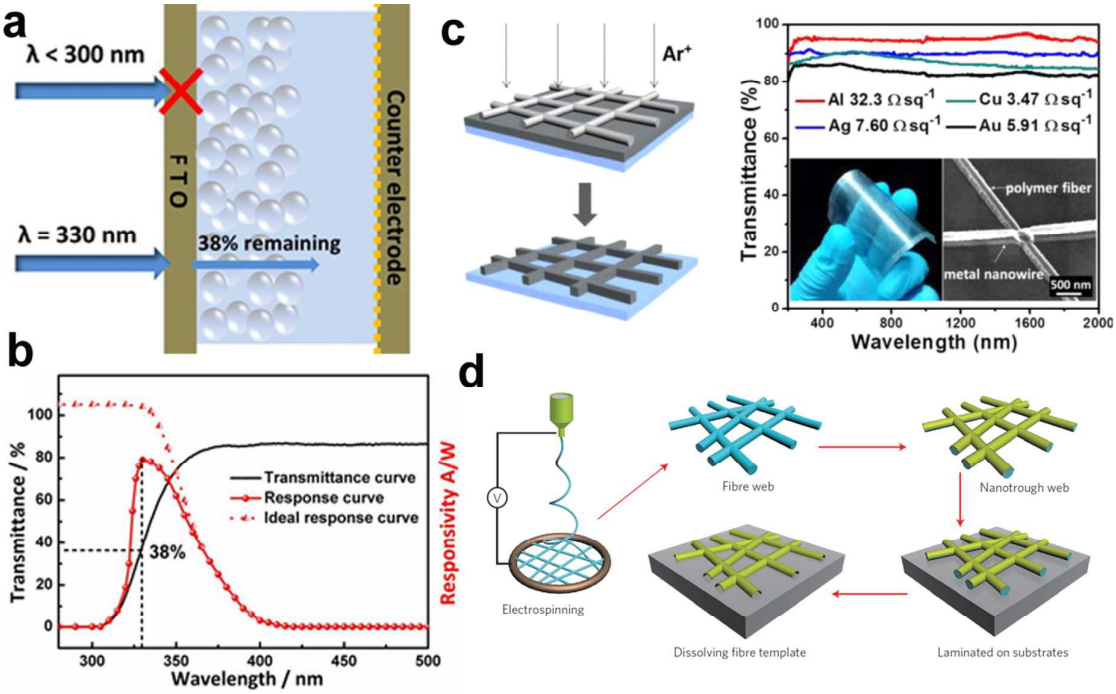

Fig. 15 (a) Schematic of UV light enter a PEC PDs using FTO as electrode connectors, (b) Typical transmittance spectrum of FTO glass (black solid line), experimental spectral response of PEC UV-PDs (red solid line), and ideal spectral response of a PEC UV-PD (red dotted line). (c) (left) Schematic in situ fabrication of a metal NW network via ion beam etching process using a polymer NF network as the shadow mask, and (right) optical transmission spectra of flexible metal networks. (d) Schematic of the polymer-NF templating process for fabricating nanotroughs. (c) Reproduced from ref. 124. Copyright© 2015 American Chemical Society. (d) Reproduced from ref. 125. Copyright© 2013, Nature Publishing Group.

Device configuration So far, most of the reported PEC UV-PDs possess a sandwich device configuration similar to a DSSC, as shown in Fig. 15a. In this configuration, TCO glass (such as FTO and ITO) is used as transparent conductive substrate, which supports the photoanode materials. Once the devices work on, the target light should enter from the side of the photoanode through the TCO glass, and then excite the semiconductor materials. However, not all UV light can transmit TCO glass easily. According to our tests, as shown in Fig. 15b (black solid line), UV light with wavelength less than 300 nm cannot transmit through TCO glass, and the one with wavelength larger than 330 nm just remain only 38% in intensity after transmission. These facts will inevitably lead to a serious issue, i.e., most of the reported PEC

UV-PDs exhibits a peak response with a full width at half maximum of about 40 nm in the range of 300-400 nm and a very low peak value in spectral responsivity at 330 nm, as shown in Fig. 15b (red solid line). If the filtering effect on the UV light source from the substrate material can be removed, the performances of PEC UV-PDs will be greatly improved. More interesting, the response spectrum will broaden, showing an ideal response curve similar to the red dotted line shown in Fig. 15b. Thus, it is very urgent to solve this "UV-filtering" problem. Some potential approaches are summarized as following:

i) To design a novel UV transparent conductive substrate to replace the traditional TCO glass. For instance, Bao *et al*. have prepared a type of transparent conductive substrate based on metal NW mesh by in-situ etching (Fig. 15c),[124] which show ~90% in transmittance within a ultra wide wave range of 200-2000 nm, and a very low resistance (2.2 Ω sq^{-1}). Moreover, Cui's group prepared metal NW mesh via sputtering or evaporation method using electrospun NWs as templates (Fig. 15d), which show sheet resistance of ~2 Ω sq^{-1} at 90% transmission.[125] However, when applied into PEC UV-PDs, these new transparent conductive substrates will meet some troubles, i.e., how to well contact the semiconductor photoanode films with the conductive layer, and how to conduct a low-temperature sintering of semiconductor films because the melting point of metal NWs is usually very low.

ii) Another effective approach is to design a type of planar device structure, i.e., put the semiconductor photoanode and counter electrode on the same substrate, which are separated via some special method such as interdigital electrode or fiber devices. And then the electrolyte will be perfused between them, and the light source can enter from the surface UV transparent window without any loss.

Material/band-gap adjustable and deep-UV detectors The newly-reported PEC UV-PDs are mainly based on the ZnO, TiO_2 and SnO_2, which have been widely used in PEC devices. However, there exist some drawbacks in those semiconductors, such as low electron

mobility, poor stability and so on. Thus, it is of great importance to seek more alternative materials to promote the practical application of PEC UV-PDs.

i) In fact, compared with other PEC applications such as DSSC, photocatalysis, photolysis of water, and so on, PEC UV-PDs usually show a low requirement on the crystal structure, absorptivity, and energy band position of the semiconductor nanomaterials. And many wide-band-gap semiconductor oxide, nitride and sulfide can be selected for their photoanode materials. For instance, GaN possesses a wide-band-gap of 3.4 eV, high electron mobility of 900 cm^2 V^{-1} s^{-1}, and high UV radiation stability, which will make it high potential into applications of PEC UV-PDs.[126] Besides, many ternary inorganic compounds with a perovskite structure, such as $SrTiO_3$ (3.15 eV), $CaTiO_3$ (3.6 eV), $BaTiO_3$ (3.3 eV) show excellent behaviors in the field of DSSC, and it is believed that these materials might also play a good role in PEC UV-PDs.

ii) For practical application, it often requires that UV-PDs possess tunable detecting cutoff wavelength, which can be realized by adjusting the semiconductors' band gap. And this idea has been widely reported and realized in the photoconductors. For instance, some ternary alloy semiconductors such as ZnMgO,[127] AlGaN[128], and so on, show a good ability in band-gap modulation, and have successfully covered the wave range from 200 to 365 nm via the component ratios. However, little similar work has been focused PEC UV-PDs up till now. And it is worth noting that the energy band structure of the semiconductor used in PEC UV-PDs should be well matched with the redox potential of the chosen electrolyte. In addition, the wetting property between semiconductor and the used electrolyte is another important issue that can greatly influence the electrolyte ion diffusion, thus determine the charge collecting efficiency.

iii) Deep-UV detectors have many important applications in military, space, and other fields. At present, photoconductor-/Schottky-type deep-UV detectors based on ultra

wide-band-gap semiconductors often exhibit a low performances. Thus, it's instructive and interesting for researchers to explore PEC deep-UV detectors.

Stabilities of PEC UV-PDs Running stability is one important indicator for the practical applications of a device. Also the stability of PEC UV-PDs is an essential issue that we should pay attention to. However, little work has reported a systematical study on the running stability of PEC UV-PDs. As well known, compared to the solid UV-PDs based on photoconductance (p-n or Schottky junctions), PEC ones usually show a worse stability, which is mainly due to the volatilization of the electrolyte (depending on the packaging process), the corrosion and surface passivation of the semiconductor, the gas generation during the work process, the decreased catalytic ability of the counter electrode (such as Pt), and so on. Thus, in view of the above points, some future work should be conducted to improve the stability of PEC UV-PDs. For instance, Chen's group attempted a nanostructured quasi-solid-state UV-PDs fabricated using a liquid LC-embedded I^-/I_3^- electrolyte, and obtained improved light harvesting and stability.[33] Further more fine long-term stability is still on the way.

Multi-functional PEC UV-PDs Recent reports on flexible, visual, and multi-functional UV-PDs with BPEs have just give an initial attempt or proposed a prototype, and further development on multi-functional detectors will significantly broaden the application fields of PEC UV-PDs. On the other hand, compared to the PDs based on metal-semiconductor-metal structure of bulky semiconductor materials, PEC UV-PD is based on nanomaterial and an electrolyte system, which showing a greater potential in flexible applications. As demonstrated, this new type of UV-PDs can work in the electrolyte of "non-toxic, environmental-friendly and cheap" water, which make the devices safer to a large extent. Moreover, it is speculative that interval replacement and filling of the water electrolyte in the devices can easily realize their circular utilization. Therefore, in brief, due to their advantages

including cheap, environmental protecting, self-powered, repeatable, and future multi-functional, it is believed that these PEC UV-PDs will have a great potential in various civilian application fields, such as medical and health protection, and wearable devices in the future.

Acknowledgements

The authors acknowledge the financial support from the National Natural Science Foundation of China (Grant Nos. 51202100 and 61404065). And the authors also thank for the great contribution from Drs. Xiaodong Li and Caitian Gao that had graduated from our group.

References

1 E. Monroy, F. Omnès and F. Calle, *Semicond. Sci. Technol.*, 2003, **18**, R33.

2 G. Shen and D. Chen, *Recent Pat. Nanotechnol.*, 2010, **4**, 20-31.

3 C. L. Hsu and S. J. Chang, *Small*, 2014, **10**, 4562-4585.

4 Z. Alaie, S. Mohammad Nejad and M. H. Yousefi, *Mater. Sci. Semicond. Process.*, 2015, **29**, 16-55.

5 G. Konstantatos and E. H. Sargent, *Nat. Nanotechnol.*, 2010, **5**, 391-400.

6 J. Zou, Q. Zhang, K. Huang and N. Marzari, *J. Phys. Chem. C*, 2010, **114**, 10725-10729.

7 C. Soci, A. Zhang, B. Xiang, S. A. Dayeh, D. P. R. Aplin, J. Park, X. Y. Bao, Y. H. Lo and D. Wang, *Nano Lett.*, 2007, **7**, 1003-1009.

8 Y. Han, G. Wu, M. Wang and H. Chen, *Polymer*, 2010, **51**, 3736-3743.

9 W. Tian, C. Zhang, T. Zhai, S. L. Li, X. Wang, M. Liao, K. Tsukagoshi, D. Golberg and Y. Bando, *Chem. Commun.*, 2013, **49**, 3739-3741.

10 X. Wang, Z. Xie, H. Huang, Z. Liu, D. Chen and G. Shen, *J. Mater. Chem.*, 2012, **22**, 6845-6850.

11 M. Gratzel, *Nature*, 2001, **414**, 338-344.

12 C. Basant, P. Leela Srinivas, K. Salaru Baba and C. N. R. Rao, *Jpn. J. Appl. Phys.*, 2011, **50**, 100206.

13 C. W. Litton, D. C. Reynolds, T. C. Collins, J. Zhong and Y. Lu, in *Zinc Oxide Materials for Electronic and Optoelectronic Device Applications*, eds. P. Capper, S. Kasap and A. Willoughby, Wiley, 2011, vol. 11, p. 363.

14 S. Sawyer and D. Shao, in *Handbook of Nanomaterials Properties*, eds. B. Bhushan, D. Luo, S. R. Schricker, W. Sigmund and S. Zauscher, Springer Berlin Heidelberg, 2014, pp. 1177-1198.

15 Y. Li, F. D. Valle, M. Simonnet, I. Yamada and J. J. Delaunay, *Appl. Phys. Lett.*, 2009, **94**, 023110.

16 S. Liu, J. Ye, Y. Cao, Q. Shen, Z. Liu, L. Qi and X. Guo, *Small*, 2009, **5**, 2371-2376.

17 F. Fang, J. Futter, A. Markwitz and J. Kennedy, *Nanotechnology*, 2009, **20**, 245502.

18 W. W. J Liu, S Bai, Y Qin, *ACS Appl. Mater. Interfaces*, 2011, **3**, 4197–4200.

19 B. Liu, Z. Wang, Y. Dong, Y. Zhu, Y. Gong, S. Ran, Z. Liu, J. Xu, Z. Xie, D. Chen, et al., *J. Mater. Chem.*, 2012, **22**, 9379-9384.

20 Y. Q. Bie, Z. M. Liao, H. Z. Zhang, G. R. Li, Y. Ye, Y. B. Zhou, J. Xu, Z. X. Qin, L. Dai and D. P. Yu, *Adv. Mater.*, 2011, **23**, 649-653.

21 W. Jin, Y. Ye, L. Gan, B. Yu, P. Wu, Y. Dai, H. Meng, X. Guo and L. Dai, *J. Mater. Chem.*, 2012, **22**, 2863-2867.

22 X. Li, C. Gao, H. Duan, B. Lu, X. Pan and E. Xie, *Nano Energy*, 2012, **1**, 640-645.

23 Y. Q. Bie, Z. M. Liao, H. Z. Zhang, G. R. Li, Y. Ye, Y. B. Zhou, J. Xu, Z. X. Qin, L. Dai and D. P. Yu, *Adv. Mater.*, 2011, **23**, 649-653.

24 S. M. Hatch, J. Briscoe and S. Dunn, *Adv. Mater.*, 2013, **25**, 867-871.

25 Q. Yang, Y. Liu, Z. Li, Z. Yang, X. Wang and Z. L. Wang, *Angew. Chem.*, 2012, **124**,

6549-6552.

26 Z. Zhan, L. Zheng, Y. Pan, G. Sun and L. Li, *J. Mater. Chem.*, 2012, **22**, 2589-2595.

27 X. Hu, B. Heng, X. Chen, B. Wang, D. Sun, Y. Sun, W. Zhou and Y. Tang, *J. Power Sources*, 2012, **217**, 120-127.

28 X. Li, C. Gao, H. Duan, B. Lu, Y. Wang, L. Chen, Z. Zhang, X. Pan and E. Xie, *Small*, 2013, **9**, 2005–2011.

29 C. Gao, X. Li, Y. Wang, L. Chen, X. Pan, Z. Zhang and E. Xie, *J. Power Sources*, 2013, **239**, 458-465.

30 Q. Li, L. Wei, Y. Xie, K. Zhang, L. Liu, D. Zhu, J. Jiao, Y. Chen, S. Yan, G. Liu, et al., *Nanoscale Res. Lett.*, 2013, **8**, 1-7.

31 L. Chen, X. Li, Y. Wang, C. Gao, H. Zhang, B. Zhao, F. Teng, J. Zhou, Z. Zhang, X. Pan, et al., *J. Power Sources*, 2014, **272**, 886-894.

32 X. Hou, X. Wang, B. Liu, Q. Wang, Z. Wang, D. Chen and G. Shen, *ChemElectroChem*, 2014, **1**, 108-115.

33 Y. Xie, L. Wei, Q. Li, Y. Chen, H. Liu, S. Yan, J. Jiao, G. Liu and L. Mei, *Nanoscale*, 2014, **6**, 9116-9121.

34 Y. Xie, L. Wei, Q. Li, Y. Chen, S. Yan, J. Jiao, G. Liu and L. Mei, *Nanotechnology*, 2014, **25**, 075202.

35 Z. Wang, S. Ran, B. Liu, D. Chen and G. Shen, *Nanoscale*, 2012, **4**, 3350-3358.

36 Y. Xie, L. Wei, G. Wei, Q. Li, D. Wang, Y. Chen, S. Yan, G. Liu, L. Mei and J. Jiao, *Nanoscale Res. Lett.*, 2013, **8**, 188.

37 J. Xing, H. Wei, E. J. Guo and F. Yang, *J. Phys. D-Appl. Phys.*, 2011, **44**, 375104.

38 J.-K. Lee and M. Yang, *Materials Science and Engineering: B*, 2011, **176**, 1142-1160.

39 T. Majumder, J. J. L. Hmar, K. Debnath, N. Gogurla, J. N. Roy, S. K. Ray and S. P. Mondal, *J. Appl. Phys.*, 2014, **116**, 034311.

40 O. Game, U. Singh, T. Kumari, A. Banpurkar and S. Ogale, *Nanoscale*, 2013, **6**, 503–513.

41 Y. Han, C. Fan, G. Wu, H. Z. Chen and M. Wang, *J. Phys. Chem. C*, 2011, **115**, 13438-13445.

42 P. Guo, J. Jiang, S. Shen and L. Guo, *Int. J. Hydrogen Energ.*, 2013, **38**, 13097-13103.

43 W. J. Lee and M. H. Hon, *Appl. Phys. Lett.*, 2011, **99**, 251102.

44 C. Cao, C. Hu, X. Wang, S. Wang, Y. Tian and H. Zhang, *Sensor Actuat. A-Chem.*, 2011, **156**, 114-119.

45 Y. Wang, W. Han, B. Zhao, L. Chen, F. Teng, X. Li, C. Gao, J. Zhou and E. Xie, *Sol. Energ. Mat. Sol. C.*, 2015, **140**, 376-381.

46 C. W. Kim, S. P. Suh, M. J. Choi, Y. S. Kang and Y. S. Kang, *J. Mater. Chem. A*, 2013, **1**, 11820-11827.

47 C. Gao, X. Li, X. Zhu, L. Chen, Y. Wang, F. Teng, Z. Zhang, H. Duan and E. Xie, *J. Alloy. Compd.*, 2014, **616**, 510-515.

48 J. Halme, P. Vahermaa, K. Miettunen and P. Lund, *Adv. Mater.*, 2010, **22**, E210-E234.

49 J. Wu, Z. Lan, J. Lin, M. Huang, Y. Huang, L. Fan and G. Luo, *Chem. Rev.*, 2015, **115**, 2136-2173.

50 Z. Sun, L. Xu, W. Guo, B. Xu, S. Liu and F. Li, *J. Phys. Chem. C*, 2010, **114**, 5211-5216.

51 Y. H. Ng, I. V. Lightcap, K. Goodwin, M. Matsumura and P. V. Kamat, *J. Phys. Chem. Lett.*, 2010, **1**, 2222-2227.

52 Y. Zhang, X. Li, M. Feng, F. Zhou and J. Chen, *Surf. Coat. Technol.*, 2010, **205**, 2572-2577.

53 J. Lei, X. Li, W. Li, F. Sun, D. Lu and J. Yi, *Int. J. Hydrogen Energ.*, 2011, **36**, 8167-8172.

54 N. L. Tarwal, V. V. Shinde, A. S. Kamble, P. R. Jadhav, D. S. Patil, V. B. Patil and P. S. Patil, *Appl. Surf. Sci.*, 2011, **257**, 10789-10794.

55 M. Chang, L. Wu, X. Li and W. Xu, *J. Mater. Sci.Technol.*, 2012, **28**, 594-598.

56 Y. Z. Su, K. Xiao, Z. J. Liao, Y. H. Zhong, N. Li, Y. B. Chen and Z. Q. Liu, *Int. J. Hydrogen Energ.*, 2013, **38**, 15019-15026.

57 Q. Wang, X. Yang, X. Wang, M. Huang and J. Hou, *Electrochim. Acta*, 2012, **62**, 158-162.

58 A. Kongkanand, R. Martínez Domínguez and P. V. Kamat, *Nano Lett.*, 2007, **7**, 676-680.

59 Y. Li, H. Yu, W. Song, G. Li, B. Yi and Z. Shao, *Int. J. Hydrogen Energ.*, 2011, **36**, 14374-14380.

60 M. Xu, P. Da, H. Wu, D. Zhao and G. Zheng, *Nano Lett.*, 2012, **12**, 1503-1508.

61 W. Chen, Y. Qiu and S. Yang, *Phys. Chem. Chem. Phys.*, 2012, **14**, 10872-10881.

62 P. Tiwana, P. Docampo, M. B. Johnston, H. J. Snaith and L. M. Herz, *ACS Nano*, 2011, **5**, 5158-5166.

63 W. Dai, X. Pan, S. Chen, C. Chen, Z. Wen, H. Zhang and Z. Ye, *J. Mater. Chem. C*, 2014, **2**, 4606-4614.

64 S. Yang, Y. Hou, J. Xing, B. Zhang, F. Tian, X. H. Yang and H. G. Yang, *Chemistry – A European Journal*, 2013, **19**, 9366-9370.

65 J. Zhao, W. Zhang, E. Xie, Z. Liu, J. Feng and Z. Liu, *Materials Science and Engineering: B*, 2011, **176**, 932-936.

66 B. Liu, X. Zhao, C. Terashima, A. Fujishima and K. Nakata, *Phys. Chem. Chem. Phys.*, 2014, **16**, 8751-8760.

67 T. Zhai, L. Li, X. Wang, X. Fang, Y. Bando and D. Golberg, *Adv. Funct. Mater.*, 2010, **20**, 4233-4248.

68 H. Xue, X. Kong, Z. Liu, C. Liu, J. Zhou, W. Chen, S. Ruan and Q. Xu, *Appl. Phys. Lett.*, 2007, **90**, 201118.

69 J. M. Macak, H. Tsuchiya, L. Taveira, S. Aldabergerova and P. Schmuki, *Angew. Chem. Int. Edit.*, 2005, **44**, 7463-7465.

70 I. S. Cho, Z. Chen, A. J. Forman, D. R. Kim, P. M. Rao, T. F. Jaramillo and X. Zheng,

Nano Lett., 2011, **11**, 4978-4984.

71 W. Q. Wu, B. X. Lei, H. S. Rao, Y. F. Xu, Y. F. Wang, C. Y. Su and D. B. Kuang, *Scientific Reports*, 2013, **3**, 1352.

72 W. Q. Wu, H. S. Rao, H. L. Feng, X. D. Guo, C. Y. Su and D. B. Kuang, *J. Power Sources*, 2014, **260**, 6-11.

73 J. Xu, Z. Chen, J. A. Zapien, C. S. Lee and W. Zhang, *Adv. Mater.*, 2014, **26**, 5337-5367.

74 T. Zhai, L. Li, Y. Ma, M. Liao, X. Wang, X. Fang, J. Yao, Y. Bando and D. Golberg, *Chem. Soc. Rev.*, 2011, **40**, 2986-3004.

75 Q. Zhang and G. Cao, *Nano Today*, 2011, **6**, 91-109.

76 M. Law, L. E. Greene, J. C. Johnson, R. Saykally and P. Yang, *Nat. Mater.*, 2005, **4**, 455-459.

77 L. Li, T. Zhai, Y. Bando and D. Golberg, *Nano Energy*, 2012, **1**, 91-106.

78 S. H. Ko, D. Lee, H. W. Kang, K. H. Nam, J. Y. Yeo, S. J. Hong, C. P. Grigoropoulos and H. J. Sung, *Nano Lett.*, 2011, **11**, 666-671.

79 M. J. Bierman and S. Jin, *Energy Environ. Sci.*, 2009, **2**, 1050.

80 X. Sun, Q. Li, J. Jiang and Y. Mao, *Nanoscale*, 2014, **6**, 8769-8780.

81 C. Gao, X. Li, B. Lu, L. Chen, Y. Wang, F. Teng, J. Wang, Z. Zhang, X. Pan and E. Xie, *Nanoscale*, 2012, **4**, 3475-3481.

82 X. Hou, B. Liu, X. Wang, Z. Wang, Q. Wang, D. Chen and G. Shen, *Nanoscale*, 2013, **5**, 7831-7837.

83 J. C. Fu, J. L. Zhang, Y. Peng, C. H. Zhao, Y. M. He, Z. X. Zhang, X. J. Pan, N. J. Mellors and E. Q. Xie, *Nanoscale*, 2013, **5**, 12551-12557.

84 N. K. Elumalai, R. Jose, P. S. Archana, V. Chellappan and S. Ramakrishna, *J. Phys. Chem. C*, 2012, **116**, 22112-22120.

85 S. Mridha, M. Nandi, A. Bhaumik and D. Basak, *Nanotechnology*, 2008, **19**, 275705.

86 B. Hu, Q. Tang, B. He, L. Lin and H. Chen, *J. Power Sources*, 2014, **267**, 445-451.

87 L. Chen, X. Li, L. Qu, C. Gao, Y. Wang, F. Teng, Z. Zhang, X. Pan and E. Xie, *J. Alloy. Compd.*, 2014, **586**, 766-772.

88 C. Xu, J. Wu, U. V. Desai and D. Gao, *J. Am. Chem. Soc.*, 2011, **133**, 8122-8125.

89 Z. Wang, H. Wang, B. Liu, W. Qiu, J. Zhang, S. Ran, H. Huang, J. Xu, H. Han, D. Chen, et al., *ACS Nano*, 2011, **5**, 8412-8419.

90 Y. Hu, X. Yan, X. Chen, Z. Bai, Z. Kang, F. Long and Y. Zhang, *Appl. Surf. Sci.*, 2015, **339**, 122–127.

91 R. S. Selinsky, Q. Ding, M. S. Faber, J. C. Wright and S. Jin, *Chem. Soc. Rev.*, 2013, **42**, 2963-2985.

92 S. Hernández, V. Cauda, D. Hidalgo, V. Farías Rivera, D. Manfredi, A. Chiodoni and F. C. Pirri, *J. Alloy. Compd.*, 2014, **615**, S530-S537.

93 M. Wang, C. Huang, Y. Cao, Q. Yu, Z. Deng, Y. Liu, Z. Huang, J. Huang, Q. Huang, W. Guo, et al., *J. Phys. D-Appl. Phys.*, 2009, **42**, 155104.

94 M. Wang, Y. Wang and J. Li, *Chem. Commun.*, 2011, **47**, 11246.

95 S. Panigrahi and D. Basak, *Nanoscale*, 2011, **3**, 2336-2341.

96 S. H. Ahn, D. J. Kim, W. S. Chi and J. H. Kim, *Adv. Mater.*, 2013, **25**, 4893–4897.

97 U. V. Desai, C. Xu, J. Wu and D. Gao, *J. Phys. Chem. C*, 2013, **117**, 3232-3239.

98 C. Gao, X. Li, X. Zhu, L. Chen, Z. Zhang, Y. Wang, Z. Zhang, H. Duan and E. Xie, *J. Power Sources*, 2014, **264**, 15-21.

99 J. Qian, P. Liu, Y. Xiao, Y. Jiang, Y. Cao, X. Ai and H. Yang, *Adv. Mater.*, 2009, **21**, 3663-3667.

100 A. Thapa, J. Zai, H. Elbohy, P. Poudel, N. Adhikari, X. Qian and Q. Qiao, *Nano Res.*, 2014, **7**, 1154-1163.

101 W. P. Liao and J. J. Wu, *J. Mater. Chem.*, 2011, **21**, 9255.

102 Y. F. Wang, K. N. Li, W. Q. Wu, Y. F. Xu, H. Y. Chen, C. Y. Su and D. B. Kuang, *RSC Adv.*, 2013, **3**, 13804-13810.

103 C. Yao, B. Wei, H. Ma, H. li, L. Meng, X. Zhang and Q. Gong, *J. Power Sources*, 2013, **237**, 295-299.

104 F. Zuo, L. Wang, T. Wu, Z. Zhang, D. Borchardt and P. Feng, *J. Am. Chem. Soc.*, 2010, **132**, 11856-11857.

105 X. Zhang, H. Tian, X. Wang, G. Xue, Z. Tian, J. Zhang, S. Yuan, T. Yu and Z. Zou, *Mater. Lett.*, 2013, **100**, 51-53.

106 Q. Zhang, L. Wang, J. Feng, H. Xu and W. Yan, *Phys. Chem. Chem. Phys.*, 2014, **16**, 23431-23439.

107 I. Justicia, P. Ordejón, G. Canto, J. L. Mozos, J. Fraxedas, G. A. Battiston, R. Gerbasi and A. Figueras, *Adv. Mater.*, 2002, **14**, 1399-1402.

108 I. S. Cho, C. H. Lee, Y. Feng, M. Logar, P. M. Rao, L. Cai, D. R. Kim, R. Sinclair and X. Zheng, *Nat. Commun.*, 2013, **4**, 1723.

109 Y. Gai, J. Li, S. S. Li, J. B. Xia and S. H. Wei, *Phys. Rev. Lett.*, 2009, **102**, 036402.

110 D. Wen, S. Guo, Y. Wang and S. Dong, *Langmuir*, 2010, **26**, 11401-11406.

111 Y. C. Pu, G. Wang, K. D. Chang, Y. Ling, Y. K. Lin, B. C. Fitzmorris, C. M. Liu, X. Lu, Y. Tong, J. Z. Zhang, et al., *Nano Lett.*, 2013, **13**, 3817-3823.

112 H. Dong, Z. Wu, F. Lu, Y. Gao, A. El-Shafei, B. Jiao, S. Ning and X. Hou, *Nano Energy*, 2014, **10**, 181-191.

113 F. Teng, G. Zhang, Y. Wang, C. Gao, L. Chen, P. Zhang, Z. Zhang and E. Xie, *Appl. Surf. Sci.*, 2014, **320**, 703-709.

114 X. An, F. Teng, Z. Zhang, X. Pan, J. Zhou and E. Xie, *Electronic Materials Letters*, 2014, **10**, 95-99.

115 F. Xu, J. Chen, X. Wu, Y. Zhang, Y. Wang, J. Sun, H. Bi, W. Lei, Y. Ni and L. Sun, *J.*

Phys. Chem. C, 2013, **117**, 8619–8627.

116 W. Wang, Q. Zhao, H. Li, H. Wu, D. Zou and D. Yu, *Adv. Funct. Mater.*, 2012, **22**, 2775-2782.

117 L. Han, L. Bai and S. Dong, *Chem. Commun.*, 2014, **50**, 802-804.

118 H. W. Chen, C. Y. Hsu, J. G. Chen, K. M. Lee, C. C. Wang, K. C. Huang and K. C. Ho, *J. Power Sources*, 2010, **195**, 6225-6231.

119 T. Miyasaka and T. N. Murakami, *Appl. Phys. Lett.*, 2004, **85**, 3932-3934.

120 Z. Yang, L. Li, Y. Luo, R. He, L. Qiu, H. Lin and H. Peng, *J. Mater. Chem. A*, 2013, **1**, 954-958.

121 T. Chen, L. Qiu, Z. Yang, Z. Cai, J. Ren, H. Li, H. Lin, X. Sun and H. Peng, *Angew. Chem. Int. Edit.*, 2012, **51**, 11977-11980.

122 J. Xu, H. Wu, L. Lu, S.-F. Leung, D. Chen, X. Chen, Z. Fan, G. Shen and D. Li, *Adv. Funct. Mater.*, 2014, **24**, 1840-1846.

123 L. Sun, X. Wang, K. Zhang, J. Zou, Z. Yan, X. Hu and Q. Zhang, *Nano Energy*, 2015, **15**, 445-452.

124 C. Bao, J. Yang, H. Gao, F. Li, Y. Yao, B. Yang, G. Fu, X. Zhou, T. Yu, Y. Qin, et al., *ACS Nano*, 2015, **9**, 2502-2509.

125 H. Wu, D. Kong, Z. Ruan, P.-C. Hsu, S. Wang, Z. Yu, T. J. Carney, L. Hu, S. Fan and Y. Cui, *Nat. Nanotechnol.*, 2013, **8**, 421-425.

126 M. Zhang, Y. Wang, F. Teng, L. Chen, J. Li, J. Zhou, X. Pan and E. Xie, *Mater. Lett.*, 2016, **162**, 117-120.

127 K. Yudai, K. Toshiyuki, N. Hiroyuki and F. Shizuo, *Jpn. J. Appl. Phys.*, 2006, **45**, L857.

128 A. Osinsky, S. Gangopadhyay, B. W. Lim, M. Z. Anwar, M. A. Khan, D. V. Kuksenkov and H. Temkin, *Appl. Phys. Lett.*, 1998, **72**, 742-744.